Data-Driven Gap Filling and Spatio-Temporal Filtering of the GRACE and GRACE-FO Records

Louis-marie Gauer, Kristel Chanard, Luce Fleitout

JGR Solid Earth

RESEARCH ARTICLE
10.1029/2022JB025561

Data-Driven Gap Filling and Spatio-Temporal Filtering of the GRACE and GRACE-FO Records

Louis-Marie Gauer[1], **Kristel Chanard**[1], **and Luce Fleitout**[2]

[1]Institut de Physique du Globe de Paris, CNRS, IGN, Université de Paris-Cité, Paris, France, [2]Laboratoire de Géologie, École Normale Supérieure, CNRS, Université PSL, Paris, France

Key Points:

- Gap filling and spatio-temporal filtering of the Gravity Recovery And Climate Experiment/Gravity Recovery And Climate Experiment Follow On gravity fields are performed using Multichannel Singular Spectrum Analysis
- The Lobe-Edge spectral filter, which complements the widely used DDK decorrelation filter, helps reducing striping noise
- The final solution shows minimal noise content and potential for retrieving smaller scale signals compared to other solutions

Supporting Information:

Supporting Information may be found in the online version of this article.

Correspondence to:

L.-M. Gauer,
gauer@ipgp.fr

Citation:

Gauer, L.-M., Chanard, K., & Fleitout, L. (2023). Data-driven gap filling and spatio-temporal filtering of the GRACE and GRACE-FO records. *Journal of Geophysical Research: Solid Earth*, *128*, e2022JB025561. https://doi.org/10.1029/2022JB025561

Received 6 SEP 2022
Accepted 23 APR 2023

Author Contributions:

Conceptualization: Louis-Marie Gauer, Kristel Chanard, Luce Fleitout
Data curation: Louis-Marie Gauer, Kristel Chanard, Luce Fleitout
Formal analysis: Louis-Marie Gauer, Kristel Chanard, Luce Fleitout
Funding acquisition: Kristel Chanard
Investigation: Louis-Marie Gauer, Kristel Chanard, Luce Fleitout
Methodology: Louis-Marie Gauer, Kristel Chanard, Luce Fleitout

Abstract Gravity Recovery And Climate Experiment and Follow On (GRACE/-FO) global monthly measurements of Earth's gravity field have led to significant advances in quantifying mass transfer. However, a significant temporal gap between missions hinders evaluating long-term mass variations. Moreover, instrumental and processing errors translate into large non-physical North-South stripes polluting geophysical signals. We use Multichannel Singular Spectrum Analysis (M-SSA) to overcome both issues by exploiting spatio-temporal information of Level-2 GRACE/-FO solutions, filtered using the DDK7 decorrelation and a new complementary filter, built based on the residual noise between fully processed data and a parametric fit to observations. Using an iterative M-SSA on Equivalent Water Height (EWH) time series processed by Center of Space Research, GeoForschungsZentrum, Institute of Geodesy at Graz University of Technology, and Jet Propulsion Laboratory, we replace missing data and outliers to obtain a combined evenly sampled solution. Then, we apply M-SSA to retrieve common signals between each EWH time series and its same-latitude neighbors to further reduce residual spatially uncorrelated noise. Comparing GRACE/-FO M-SSA solution with Satellite Laser Ranging and Swarm low-degree Earth's gravity field and hydrological model demonstrates its ability to satisfyingly fill missing observations. Our solution achieves a noise level comparable to mass concentration (mascon) solutions over oceans (3.0 mm EWH), without requiring a priori information nor regularization. While short-wavelength signals are challenging to capture using highly filtered spherical harmonics or mascons solutions, we show that our technique efficiently recovers localized mass variations using well-documented mass transfers associated with reservoir impoundments.

Plain Language Summary The Gravity Recovery and Climate Experiment and Follow-On (GRACE/-FO) satellite global measurements of changes in the Earth gravity field uniquely observe mass variations within and between the atmosphere, oceans, continental hydrology and ice. Yet, monthly data are polluted by noise in a North/South striping pattern, likely related to systematic errors and imperfect correction models. Moreover, the gap between missions hinders quantifying mass changes rates, which is essential for measuring and understanding the impacts of climate change and human activity on the evolving ice and freshwater resources. To overcome both issues, we present a new post-processing procedure of the GRACE/GRACE-FO gravity fields, that has potential for an improved spatial resolution. This is accomplished using a mathematical method that exploits spatio-temporal correlations in the gravity time series. We perform gap filling based on the most statistically correlated signals and efficiently filter gravity fields by discarding the less correlated ones. The final GRACE/GRACE-FO solution shows low residual noise level over the oceans and is able to retrieve short-wavelengths signals such as reservoir impoundments or small glaciers, which are often smeared out over large regions or masked out by other processing methods.

1. Introduction

From March 2002 to October 2017, the Gravity Recovery And Climate Experiment (GRACE) has measured changes in the Earth's gravity field (Tapley et al., 2004). The GRACE mission included two satellites in a low, near-circular, near-polar orbit following each other at a distance of approximately 220 km. When the leading satellite passed over a sizable mass, it was pulled slightly more toward the mass than the trailing satellite and orbits were perturbed differently. By precisely measuring variations in the intra-satellites distance, it was possible to quantify the Earth's mass variations through the differential gravitational pull on the two satellites. GRACE proved relevant and rapidly became an essential tool for monitoring the movements of mass within and between Earth's atmosphere, oceans, land and ice sheets. In fact, over the past decades, GRACE has provided insights in various fields, from geophysics to hydrology. For example, observations of mass variations derived from

Project Administration: Kristel Chanard
Resources: Louis-Marie Gauer, Kristel Chanard, Luce Fleitout
Software: Louis-Marie Gauer
Supervision: Kristel Chanard, Luce Fleitout
Validation: Louis-Marie Gauer, Kristel Chanard, Luce Fleitout
Visualization: Louis-Marie Gauer, Kristel Chanard, Luce Fleitout
Writing – original draft: Louis-Marie Gauer, Kristel Chanard, Luce Fleitout
Writing – review & editing: Louis-Marie Gauer, Kristel Chanard, Luce Fleitout

GRACE have been used to monitor global and regional terrestrial water storage (J. Chen et al., 2016; Long et al., 2015; Longuevergne et al., 2013; Syed et al., 2008), global ocean mass changes (Gardner et al., 2013; Morison et al., 2007; Wouters et al., 2011), ocean bottom pressure (Johnson & Chambers, 2013), or recent ice melting (Luthcke et al., 2013; Wouters et al., 2019). Moreover, GRACE revealed valuable information on processes occurring within the solid Earth, including the seismic cycle (Bouih et al., 2022; J. L. Chen et al., 2007; Panet et al., 2007) or Glacial Isostatic Adjustment (GIA; Steffen et al., 2008; Velicogna & Wahr, 2013). The success of the GRACE mission overall motivated a follow-up mission, GRACE-Follow On (GRACE-FO; Flechtner et al., 2016; Landerer et al., 2020), launched in May 2018. Nonetheless a significant temporal gap between the two missions exists, in addition to the increasing missing observations toward the end of the GRACE mission. Yet, having a time series of measurements of sufficient length, consistency and continuity is essential to investigate long-term gravity changes occurring with the solid Earth processes and, even more so, monitor climate-related mass variations, such as the ongoing evolution of ice sheets and glaciers or land water storage.

However, due to the orbital geometry of both missions, observations bear a low-sensitivity in the East-West direction. As a result, instrumental errors, shortcomings and inaccuracies in the oceanic and atmospheric gravity field dealiasing models (Seo et al., 2006, 2007), or any other processing error translate into a distinctive noise with a North-South striping pattern, limiting GRACE measurements quality and potential use for even more geophysical applications (Han et al., 2004; Swenson & Wahr, 2006; Thompson et al., 2004). In order to reduce this characteristic noise, several signal processing methods have been developed using various mathematical tools (Werth et al., 2009). First, North-South stripes polluting the gravity fields derived from raw GRACE observations, expressed in terms of Stokes coefficients of their Spherical Harmonics (SH) decomposition, can be removed using different filtering methods. Examples of post-processing methods include: Gaussian filters (Seo et al., 2007; Wahr et al., 2004), a combination of them (Guo et al., 2010), or the widely used DDK decorrelation filters (Kusche, 2007; Kusche et al., 2009). DDK filters aim at reducing correlations between Stokes coefficients of the gravity field SH decomposition and are provided as convolution matrices. Since all filtering methods require a compromise between smoothing—hence spatial resolution and signal attenuation—and reducing noise, DDK filters offer a family of filters (DDK1 to DDK8), corresponding to different levels of filtering. To further reduce noise in the GRACE and GRACE-FO derived gravity fields, partly due to limitations in processing strategies, solutions provided by various processing centers can be combined at the observations level (COST-G; Jäggi et al., 2020), or averaged during post-processing (Sakumura et al., 2014). Uncertainties related to solution processing and post-processing strategies can also be accounted for using an ensemble approach (Blazquez et al., 2018). Alternatively, the GRACE mass concentration (mascons) solutions have been developed to propose leakage-suppressed and ready to use solutions (Luthcke et al., 2013; Save et al., 2016; Watkins et al., 2015). However, achieving these solutions requires the introduction of potentially biased a priori information on the spatio-temporal distribution of the signal or noise structure, or regularization in the least-squares gravity inversion (Loomis et al., 2019).

In parallel, statistical signal-processing techniques, namely statistical decomposition methods, have been used to identify patterns of variability in the GRACE time series. Most of these methods aim at retaining only a set of patterns representing most of the geophysical signal variability, in order to filter out less correlated parts of the signal dominated by North-South stripes. In particular, eigenspace techniques have been commonly applied to isolate geophysical signals in GRACE derived gravity field time series. First, Principal Component Analysis (PCA; Lorenz, 1956), also called Empirical Orthogonal Function analysis, has been used to extract dominant orthogonal modes from GRACE data, either for filtering noise (Chambers, 2006; Chambers & Willis, 2008; Schrama et al., 2007; Wouters & Schrama, 2007), or extracting signals of interest (De Viron et al., 2006; Rangelova et al., 2007; Rangelova & Sideris, 2008; Rieser et al., 2010). However, the physical interpretation of modes extracted using PCA can be biased by the superposition of independent source signals in the time series. Therefore, Independent Component Analysis (ICA), which aims at separating dominant modes based on the assumed statistical independence of signal sources, has been preferred over PCA (Forootan & Kusche, 2012; Frappart et al., 2010). Yet, both PCA and ICA only use information between existing time series, ignoring the potential lagged correlations between time series, and are thus limited to stationary processes. If they are efficient at separating signals with various temporal behaviors, capturing the spatio-temporal evolving nature of geophysical signals encompassed in the GRACE data remains challenging (Forootan et al., 2014). Incorporating any lagged information on a single time series is fortunately possible using Singular Spectrum Analysis (SSA; Vianna et al., 2007; X. Wang et al., 2011). Moreover, the Multichannel (or multivariable)-SSA (M-SSA; e.g.,

Ghil et al., 2002), a generalization of both the PCA and SSA, which uses time-lagged observations and multiple time series, is particularly well adapted to capture the complex spatio-temporal modes of variability of the GRACE data and to filter processing-specific errors and noise (Prevost et al., 2019; Rangelova et al., 2012; F. Wang et al., 2020; Zotov & Shum, 2010).

The large number of missing observations toward the end of the GRACE mission and the 11-month observational gap between missions limit the potential use of GRACE and GRACE-FO data to their full potential. Consequently, efforts have been carried out to fill temporal observational gaps of the GRACE gravity fields. First, independent observations have been used to fill GRACE data gaps. Particularly, direct observations from Satellite Laser Ranging (SLR) or Global Positioning System receivers onboard Swarm satellites can be exploited to reconstruct low-degrees of the Earth's gravity field (Jäggi et al., 2016; Lück et al., 2018; Richter et al., 2021). Inversions of deformation fields, as measured for example, by Global Navigation Satellite System global networks can also lead to low-degree gravity field estimates through loading theory (Chanard et al., 2018; Rietbroek et al., 2014; Wu et al., 2020). Yet, independent data may contain specific technique-related errors or other physical processes that can bias GRACE gravity field gap filling (Dong et al., 2002; Mémin et al., 2020). GRACE temporal gaps can be reconstructed using data-adaptive statistical techniques, such as SSA and M-SSA, to decompose the time series into a subset of temporal or spatio-temporal components then used to reconstruct missing observations (Kondrashov & Ghil, 2006). SSA has been used in an iterative approach to perform gap filling on time series of the coefficients of GRACE gravity field SH decomposition (Li et al., 2019; Prevost et al., 2019; Yi & Sneeuw, 2021). M-SSA has also proven its ability to reconstruct missing observations, at least for low-degree SH coefficients of the Earth's gravity field, using Swarm observations (F. Wang et al., 2021), or part of the gravity variations, namely climate-driven water storage changes, using precipitation and temperature models (Humphrey & Gudmundsson, 2019; Yang et al., 2021). Recently, more advanced machine learning techniques have also been employed to perform gap filling in and between GRACE and GRACE-FO observational periods. Examples include reconstructing the terrestrial water component of the gravity field using an hydroclimatic data-driven Bayesian convolutional neuronal network (Mo et al., 2022) or an algorithm combining M-SSA with an artificial neural network (Lai et al., 2022). Nonetheless, these methods are more complex, computationally more challenging than classical statistical methods, and often limited to terrestrial water storage applications discarding mass change related to solid Earth processes.

In this study, we propose an improved post-processing strategy for gap filling based on previous work by Prevost et al. (2019). By combining and filtering four Level-2 GRACE and GRACE-FO gravity field solutions using a unique statistical method, the M-SSA, in a simpler yet more efficient way than Prevost et al. (2019), we propose a solution with an improved spatial resolution and minimal noise content. In the following, we first present, in Section 2, the GRACE/GRACE-FO datasets used and pre-M-SSA processings applied in this study. In Section 3, after briefly describing the M-SSA method, we explicit our post-processing strategy, in light of previous work, and present results. The method includes an iterative M-SSA algorithm for observational gap filling using multiple Level-2 GRACE and GRACE-FO solutions, with synthetic tests for validation, a new filter in the spectral domain and a M-SSA-based spatio-temporal filtering procedure to efficiently reduce the persistent North-South stripes. Then, in Section 4, we first validate the M-SSA gap filling algorithm by comparing results to independent observations, namely SLR and Swarm for low-degree SH coefficients and a hydrological model. Finally, we compare our results with published GRACE and GRACE-FO solutions, using different processing strategies. In particular, we confront noise content of the gravity field solutions over the oceans, and assess solutions performances for a selection of regional examples, including hydrological mass balance for reservoir impoundments.

2. GRACE and GRACE-FO Level-2 Solutions

2.1. GRACE and GRACE-FO Datasets

The GRACE and more recently, the GRACE-FO missions provide monthly maps of the Earth's gravity field with a spatial resolution of a few hundreds kilometers (Landerer et al., 2020; Tapley et al., 2004). But a substantial 11-month temporal gap, from June 2017 to May 2018, exists between missions (Figure S1 in Supporting Information S1). The raw Level-1 data are processed by several processing centers to provide monthly Level-2 solutions of the Earth's gravitational field. These solutions are distributed in terms of Stokes coefficients of the Earth's gravity field SH decomposition. Differences in processing strategies yield two major consequences. First, raw Level-1 monthly signal to noise ratio requirements cause differences in Level-2 temporal sampling between

processing centers (Figure S1 in Supporting Information S1). Then, noise discrepancies arise from differences in processing strategies (Sakumura et al., 2014; Swenson & Wahr, 2002). In this study, we take advantage of Level-2 gravity field solutions from four different processing centers, expressed in Stokes coefficients of the SH decomposition up to the degree 96. We focus our study on the January 2003–September 2022 period, using the available GRACE data from January 2003–June 2017 and GRACE-FO data from June 2018–September 2022, discarding here the starting period of the GRACE mission (February 2002–December 2002). Note that we discard the beginning of the GRACE mission because the post-processing method proposed in this study is mathematically more challenging when significant noise occurs at the beginning or end of the observational time series (Yi & Sneeuw, 2021). Finally, all GRACE and GRACE-FO solutions used in this study are corrected for non-tidal high-frequency atmospheric and oceanic mass variation models, namely the Atmosphere and Ocean Dealiasing Level-1B (AOD1B) model (Dobslaw et al., 2017) by the processing centers.

2.2. GRACE and GRACE-FO Data Pre-M-SSA Processing

Several pre-processing steps are required prior to using the GRACE and GRACE-FO datasets for geophysical applications. First, the non-observable degree-1 SH geocenter gravity coefficients are accounted for using the corresponding coefficients provided for each of the GeoForschungsZentrum (GFZ), Jet Propulsion Laboratory (JPL) and Center of Space Research (CSR) solutions in Technical Note 13 (TN-13; Swenson et al., 2008; Sun et al., 2016) and the average of those coefficients for the Institute of Geodezy at Graz University of Technology (GRAZ) solution. Then, $C_{2,0}$ Earth oblateness and $C_{3,0}$ gravity coefficients, which are difficult to observe due to the near polar orbit and accelerometer errors (Klinger & Mayer-Gürr, 2016), are substituted with SLR observations according to Technical Note 14 (TN-14; J. Chen et al., 2005; Loomis et al., 2020).

Moreover, to investigate variations in the Earth's gravity field, we remove its mean value estimated for each Level-2 solution over the 2003–2022 period respectively. Consequently, the characteristic nonphysical North-South elongated striping patterns, arising from instrumental errors or shortcomings in the gravity field correction models of known phenomena, dominate both GRACE and GRACE-FO solutions. Figures 1a and 1b show examples of the resulting GRACE and GRACE-FO gravity fields, expressed in Equivalent Water Height (EWH) for July 2008 and 2019 respectively. The large amplitude of the North-South striping artifacts emphasizes the necessity for filtering the GRACE and GRACE-FO gravity fields prior to any geophysical application (Sakumura et al., 2014). Here, we start by using the non-isotropic decorrelation filter, known as DDK (Kusche, 2007; Kusche et al., 2009). DDK is based on a regularization using both the error and signal covariance information. The filter results in a single filtering matrix derived from the a priori error covariance of the August 2003 GRACE solution, that we apply to all GRACE and GRACE-FO monthly gravity fields. The filter offers 8 levels, from the strongest DDK1 to weakest DDK8 level, and impacts mainly the high degree coefficients of the SH decomposition which contain most of the stripping noise. An increase in the level of DDK filtering yields larger signal attenuation and leakage causing geophysical signals to smear out over larger regions. Thus, a compromise between solution filtering and noise reduction must be made. While the choice of DDK filter depends on the application, DDK5 appears to be the most commonly used for geophysical applications and using an average of solutions has proven to reduce processing artifacts in earlier releases of Level-2 SH solutions (Sakumura et al., 2014). We thus show, as a reference solution, an example of the mean of the four solutions (CSR, JPL, GFZ, GRAZ), that we later combine to create the GRACE-MSSA solution, filtered using DDK5. DDK5 efficiently removes a large part of the North-South stripes while retaining geophysical signals, with a spatial resolution that can be compared to a 180 km Gaussian filter radius equivalent, obtained from the comparison of the isotropic part of the anisotropic DDK filters with the Gaussian ones (Cambiotti, 2020; Kusche et al., 2009; Figures 1c and 1d).

Here, we rather apply the DDK7 filter, with a spatial resolution that can be compared to a 145 km isotropic Gaussian filter radius equivalent (Figures 1e and 1f). Figure 2 shows an example of the impact of applying DDK5, compared to DDK7, on the intensity spectrum of the SH decomposition for the July 2008 GRACE CSR gravity field. DDK5 removes a larger part of the signal at high degrees which, while largely polluted by North-South striping artifacts, may still contain valuable geophysical information.

Here, we first combine the DDK7 filter with a complementary filter, the Lobe-Edge (LE) filter, for which coefficients are provided in Figure S2 in Supporting Information S1. This filter is developed based on the residual noise between fully processed data and a parametric fit to observations, to further reduce persisting stripes. A full description of the LE filter is provided in Section 3.5. All results presented in the following are based on

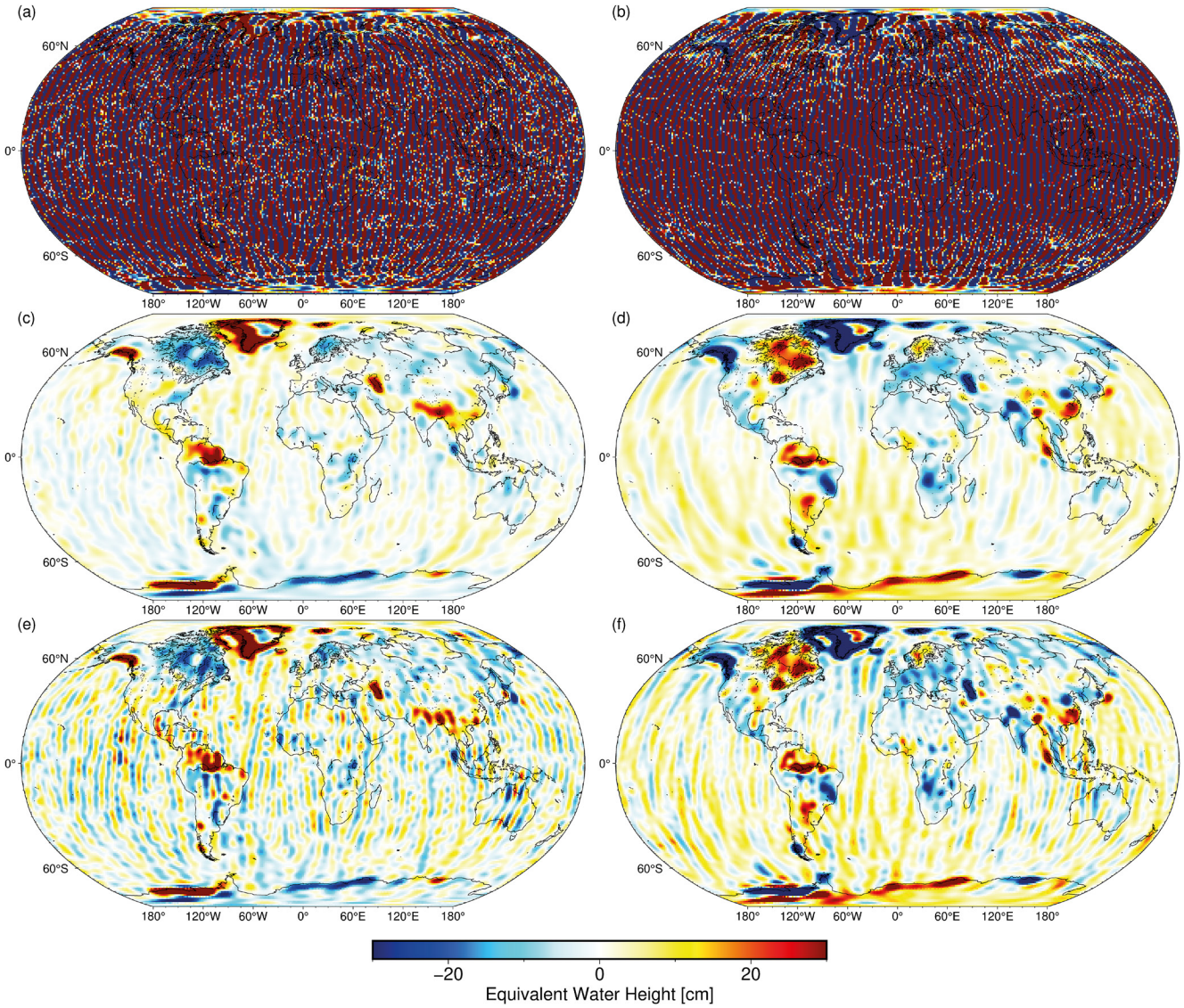

Figure 1. Mean of surface mass anomaly of the unfiltered (a) and (b), the DDK5-filtered (c) and (d), and the DDK7-filtered (e) and (f) GRACE and GRACE-FO solutions processed by the CSR, GFZ, GRAZ and JPL centers, for July 2008 and July 2019 respectively, after removing its mean value estimated for each Level-2 solution over the 2003–2022 period respectively. Surface mass anomalies are expressed in Equivalent Water Height (cm).

a DDK7 + LE filtering of the GRACE/GRACE-FO solutions, and results based on a DDK7 filtering only can be found in Supporting Information S1 undermentioned. Next, we propose to perform an additional filtering which involves no a priori information on the signal nor the noise structure. This additional filtering further reduces spurious noise while retaining smaller wavelengths signals and limits signal attenuation compared to the commonly used average of DDK5-filtered solutions (Sakumura et al., 2014). By doing so, we intend to broaden possibilities of using GRACE and GRACE-FO in various geophysical domains.

3. Methodology

Once the GRACE and GRACE-FO data have been pre-processed with DDK7 and LE filtering, solutions still contain significant North-South striping artifacts and missing data remain an issue for geophysical applications. The aim of the methodology developed in this study is to address both issues using a unique mathematical tool, namely the Multichannel-Singular Spectrum Analysis (M-SSA). In the following Section, we first briefly describe the M-SSA and then detail both steps of the proposed methodology to fill and filter the pre-processed

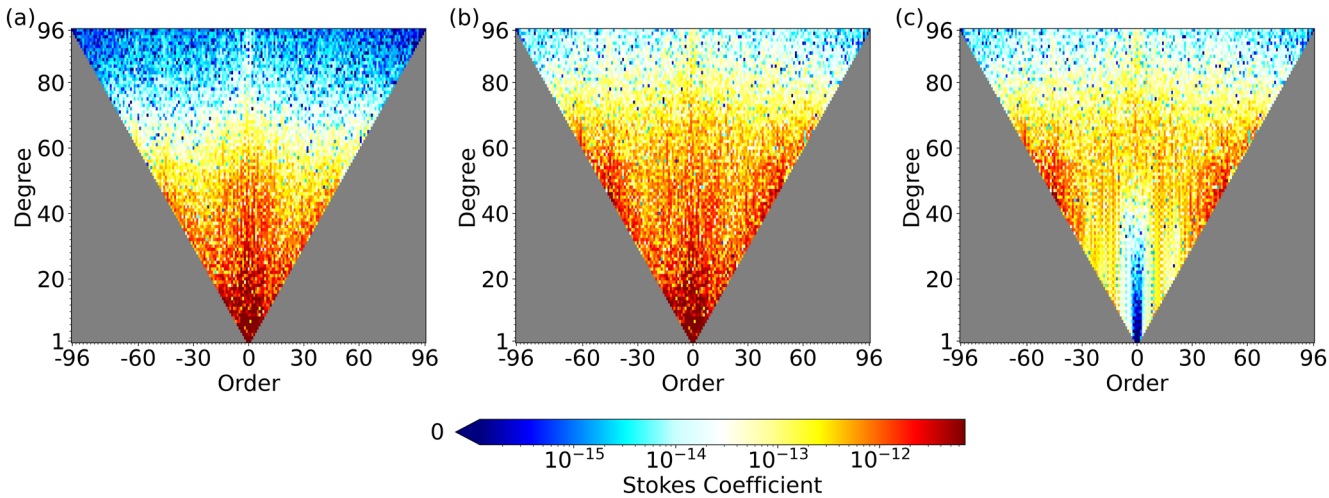

Figure 2. Stokes coefficients intensity spectra of the July 2008 GRACE CSR gravity filtered using (a) DDK5 and (b) DDK7 decorrelation filter. (c) Shows the difference between DDK7 and DDK5 filtering applied to the same July 2008 GRACE CSR gravity field.

GRACE and GRACE-FO data as objectively as possible, in light of previous work by Prevost et al. (2019) on which this procedure is based. This post-processing method is separated in two major steps: (a) data gap filling and (b) spatio-temporal filtering.

3.1. Multichannel Singular Spectrum Analysis (M-SSA)

M-SSA is a data-adaptive, non-parametric mathematical method that exploits spatial and temporal correlations associated with channels, or time series, to separate either signal from noise or signals from different origin (e.g., Ghil et al., 2002; Keppenne & Ghil, 1993; Plaut & Vautard, 1994). M-SSA decomposes time series into spatio-temporal modes of variability that can isolate nonlinear trends or oscillatory evolution from noise. These modes are derived from the eigenvectors of the covariance matrix between time series and their delayed copies. The projection of time series and their delayed copies upon the eigenvectors gives the Principal Components (PCs), that represent the temporal behavior of the determined modes of variability and are an efficient tool to identify geophysical components from noise. The variance of the mode described by each PC is given by the corresponding eigenvalues and reflect its relative importance to explain the original time series. The projection of a subset of PCs onto the eigenvectors, called Reconstructed Components (RCs), provides the opportunity to visualize the time series after filtering out low-variance components, likely associated with noise. A detailed description of the method is provided in Text S1 in Supporting Information S1. A more complete review of the methodology, including various examples of application, is given by Ghil et al. (2002).

Here, M-SSA is particularly interesting to (a) fill the GRACE and GRACE-FO data temporal gaps by simultaneously relying on the temporal evolution of EWH time series provided by several processing centers, and (b) reduce spurious uncorrelated noise in the data by retaining only the most correlated parts of the signal in space and time, without a priori information on the signal or noise structure.

3.2. An Improved GRACE/GRACE-FO M-SSA Gap Filling and Filtering Method

One of the current challenges of using GRACE and GRACE-FO data for various geophysical applications is accounting for missing observations, particularly between missions for various geophysical applications. Another important challenge is to further increase spatial resolution of the solutions while efficiently reducing their noise content. Indeed, while heavily filtered solutions lead to negligible noise, they suffer from signal amplitude attenuation and spatial leakage over large regions, which makes them unsuitable for geophysical applications such as regional mass balance. The potential of (M-)SSA for both temporal gap filling and spatio-temporal filtering of the GRACE data has previously been investigated by Prevost et al. (2019) to obtain a continuous GRACE solution with minimal noise content and maximal spatial resolution.

To do so, Prevost et al. (2019) used a 3-steps (M-)SSA based method on multiple Level 2 GRACE gravity field anomalies, previously filtered by DDK7. First, temporal gap filling was performed on time series of the SH coefficients of each GRACE solution, using an iterative SSA scheme. Then, M-SSA was used to average the evenly spaced time series of SH coefficients from several processing centers simultaneously to retain their common modes of variability, while discarding their differences. Finally, M-SSA was used as a spatio-temporal filter applied to the averaged solution, converted into a grid of EWH, to remove residual North-South stripes by taking advantage of the spatial and temporal correlations of physically driven gravity changes. Figure S3 in Supporting Information S1 shows a diagram of the method proposed by Prevost et al. (2019).

Prevost et al. (2019) constitutes the basis of the method presented here. However, extending this method to the GRACE and GRACE-FO data and improving noise reduction is challenging, requiring an improved procedure (Figure 3). First, we develop and add the LE filter to complement the DDK7 filter (see Figure S2 in Supporting Information S1 and Section 3.4). Then, we directly perform an improved gap filling using M-SSA simultaneously on EWH time series from multiple processing centers. Moreover, we proceed to outliers detection and replacement. Finally we simplify the original temporal filtering and perform gap filling on spatially distributed time series of EWH rather than on their SH equivalent (Prevost et al., 2019; F. Wang et al., 2021) in order to simplify the method overall by performing both gap filling and spatial filtering on time series of EWH. Steps of our procedure are further described in Sections 2.2, 3.3, and 3.4. Comparisons of methods performances are provided in Section 4.

3.3. Temporal Gap Filling With M-SSA

We first convert the Level-2 GRACE and GRACE-FO Stokes coefficients of the Earth's gravity field, pre-processed according to Section 2.2., for each processing center c, at each date t, into global grids of surface mass anomaly $\sigma^c(t, \lambda, \varphi)$, where, $c \in$ [CSR, GFZ, GRAZ, JPL], λ and φ are the longitude and latitude. $\sigma^c(t, \lambda, \varphi)$ is expressed in EWH. We then use a data-adaptive iterative gap-filling algorithm based on single-channel SSA (Kondrashov et al., 2010; Kondrashov & Ghil, 2006) and recently extended to (M-)SSA for GRACE and GRACE-FO applications (Prevost et al., 2019; F. Wang et al., 2020, 2021). We adopt a 3-step gap filling procedure: (a) we fill the gaps using an ordinary least squares estimation-based interpolation (including third order polynomial, annual, and semiannual terms), (b) we remove outliers using M-SSA and (c) we perform an iterative M-SSA and replace missing observations using predictions increasingly correlated with the EWH time series. Each step is further described in the following.

1. Our gap filling algorithm consists first in filling the observational gaps (Figure S1 in Supporting Information S1) for each point of geographic coordinates (λ, φ) and each solution by performing an ordinary least squares estimation-based interpolation (including third order polynomial, annual, and semiannual terms) using all provided data. An example of this interpolation of EWH is shown in Figure 4a for a point located in the Caspian sea (more examples are provided in Figure S4 in Supporting Information S1). Using an interpolation model including a third order polynomial, annual and semiannual signals allows to capture significant long term mass loss and annual variations. For instance, the variation in trend in the Caspian sea, likely due to hydrological processes, between the artificially missing 2008 years, for method validation, and the 2017–2018 inter-mission period can be better recovered (Figure 4a). Here, we choose an ordinary least squares estimation-based interpolation (including third order polynomial, annual, and semiannual terms) over a linear, mean or zero value gap filling one (Prevost et al., 2019; Walwer et al., 2016) to optimize M-SSA performances.
2. Once EWH time series are evenly spaced, thanks to the ordinary least squares estimation-based interpolation (including third order polynomial, annual, and semiannual terms), it is possible to apply the M-SSA algorithm. Nevertheless, the reconstructed data gaps by a first M-SSA are highly influenced by the entire EWH time series. Therefore, we detect and replace potential outliers, outside of data gaps, to further improve the iterative reconstruction by M-SSA and therefore, the gap filling performances. For this purpose, we start by retrieving, for EWH time series of each point of coordinates (λ, φ), the principal modes of variability of the four solutions used in this study. To do so, we perform a M-SSA analysis on the four EWH time series simultaneously, using a sliding window of $M = N/2$, where $N = 237$ is the length of the evenly sampled GRACE/GRACE-FO time series for the period considered. We retain the first 8 PCs to reconstruct the signal for each solution, that is, the first $N_c = 8$ RCs for each processing center c. A detailed analysis of M-SSA parameters selection is provided in the following for the gap filling method and also applies to outliers detection analysis. We then average the reconstructed EWH time series of all processing centers to obtain a unique mean M-SSA-based EWH time

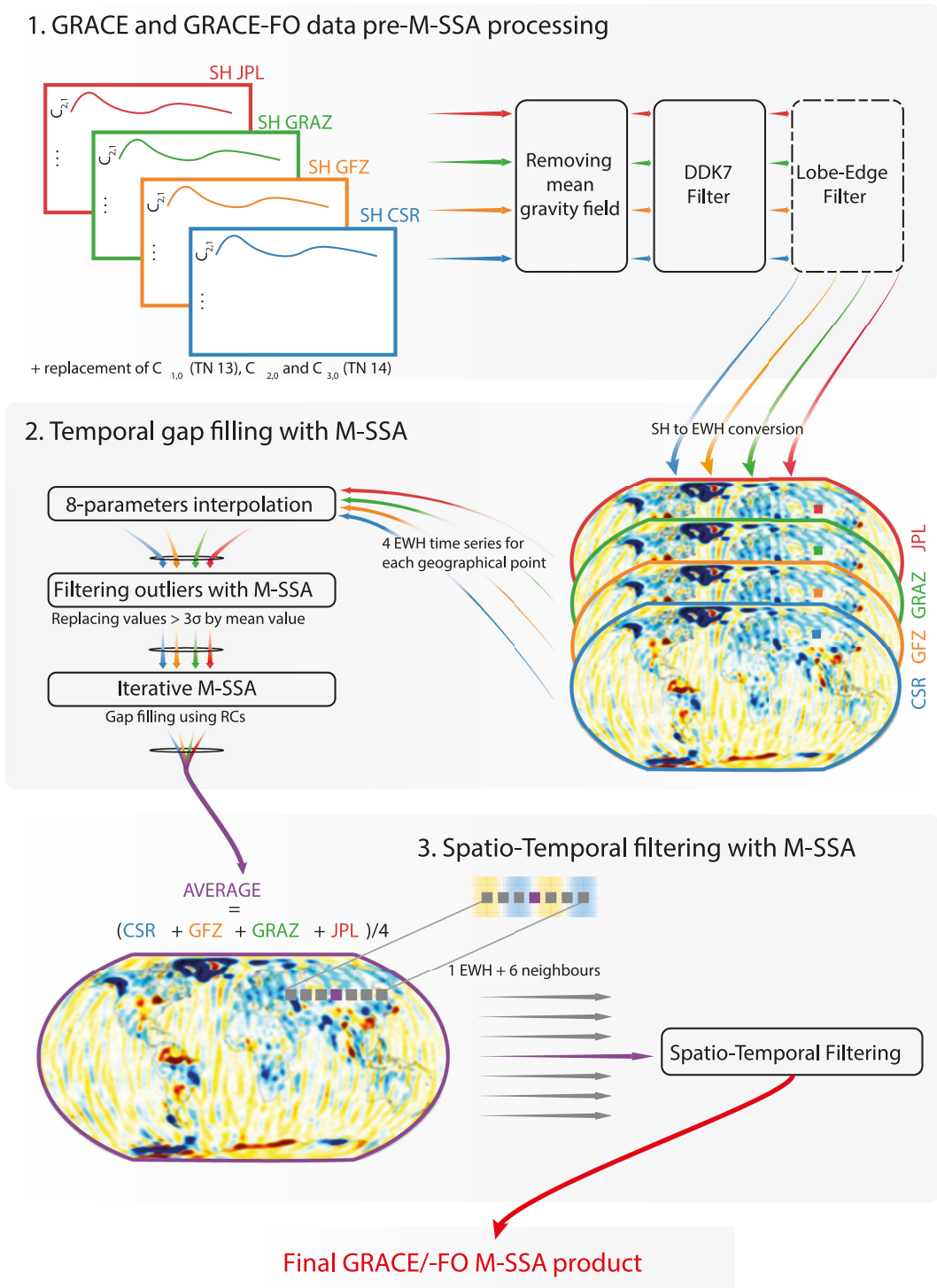

Figure 3. Diagram of the processing procedure developed in this study. The three major steps relate directly to a subsection of this article.

series, $\sigma^m_{MSSA}(t, \lambda, \varphi)$, capturing the principal modes of variability of the signal processed by the four different centers. The average is defined as:

$$\sigma^m_{MSSA}(t, \lambda, \varphi) = \frac{1}{4} \sum_{c=1}^{4} \sum_{i=1}^{8} RC^i_c(t, \lambda, \varphi), \quad (1)$$

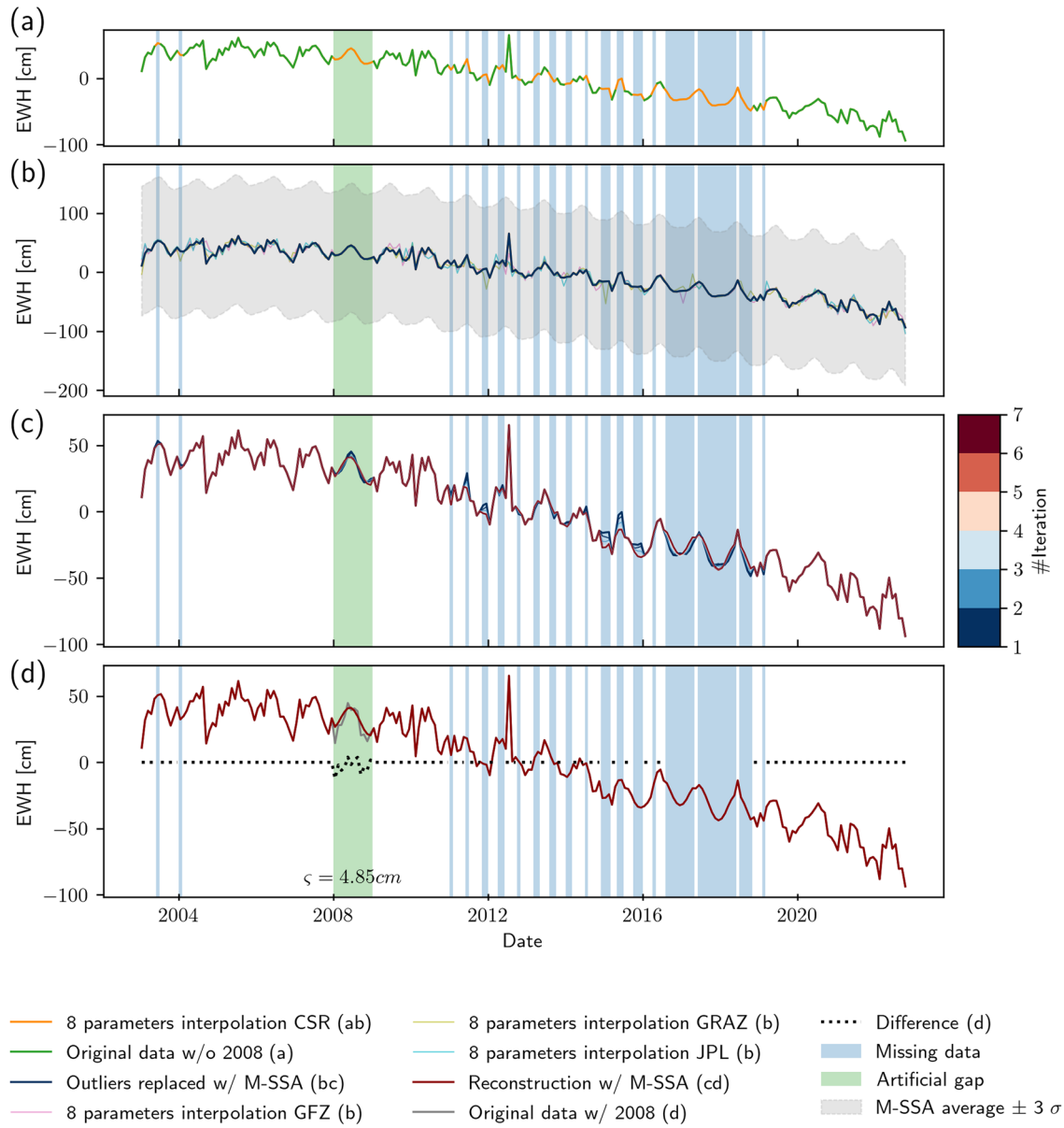

Figure 4. Example of M-SSA gap filling method for time series of CSR GRACE/GRACE-FO surface mass anomalies, expressed in Equivalent Water Height (EWH) (cm), for a point located in the Caspian Sea (51°E, 41°N). Observational gaps are highlighted in light blue while the artificial gap for method validation is shown in light green. (a) Shows the original EWH time series filtered by DDK7 and the Lobe-Edge (LE) filter (green, LE filter is presented in Section 3.5), and its evenly sampled version filled by an ordinary least squares estimation-based interpolation (including third order polynomial, annual, and semiannual terms) using all data outside of observational gaps (orange). (b) Shows EWH time series of solutions processed by CSR, GFZ, GRAZ and JPL (orange, pink, khaki and cyan) and the area corresponding to 3 times the standard deviation of a mean M-SSA based EWH time series of all solutions (light gray), which is a criterion used to identify potential outliers. When they exist (see Figure S4.2 in Supporting Information S1 for a case where outliers are removed), outliers are replaced by their mean M-SSA based EWH time series value to build a filtered version of the EWH time series (dark blue). (c) Illustrates the iterative scheme to perform gap filling (blue to red). (d) Method performance is evaluated for year 2008, artificially removed from the original dataset and reconstructed, by comparing the final reconstruction (red) with the original GRACE observations (gray). Differences between the reconstructed and original signals for year 2008 are shown in dotted black line, and Root-Mean-Square value of the difference over 1 year is provided.

where RC_l^i is the ith RC given by the M-SSA for the lth time series (see Text S1 in Supporting Information S1 for additional information).

We identify outliers in EWH time series processed by individual centers as larger than three times the standard deviation of the mean M-SSA EWH time series, σ^m_{MSSA} (see Figure S5 in Supporting Information S1 for tests on outliers detection criterion). Outliers, if they exists, are replaced by the corresponding value of σ^m_{MSSA},

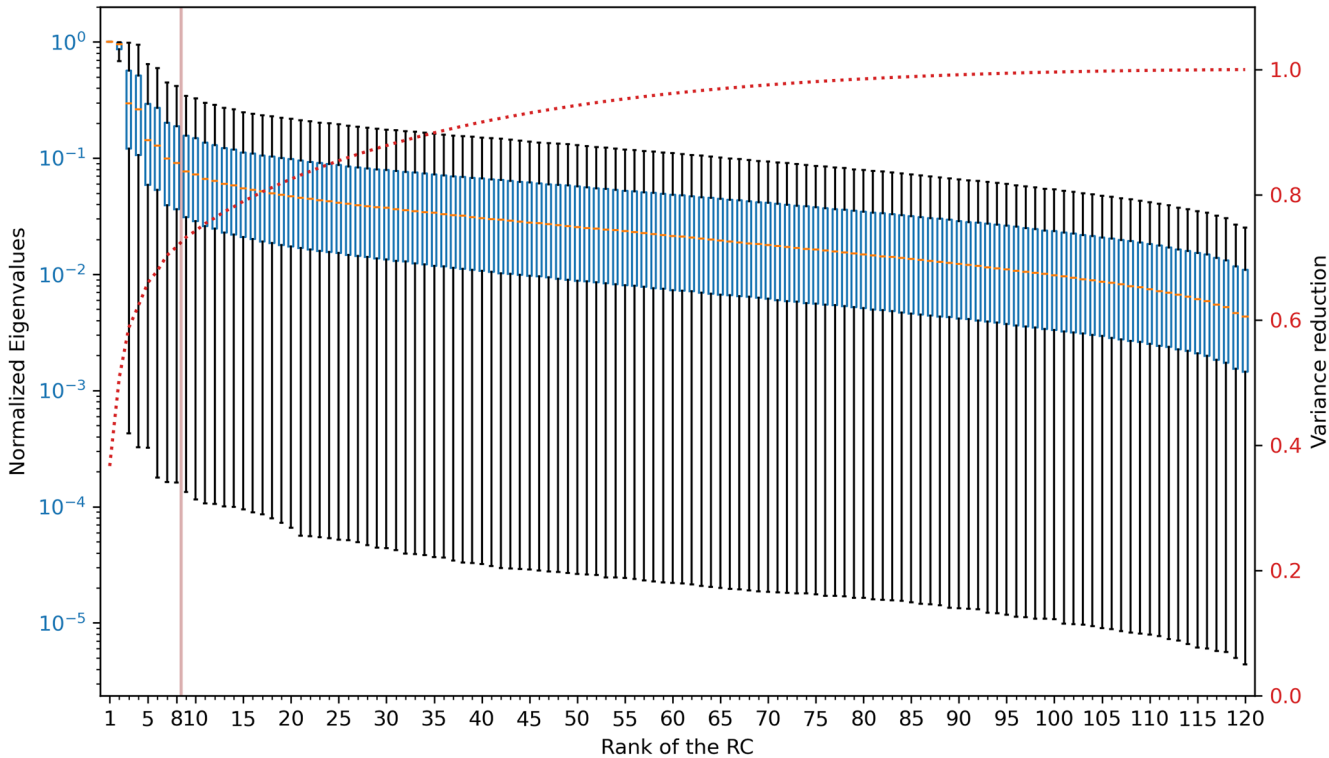

Figure 5. Normalized first 113 eigenvalues of the M-SSA analyses performed on a selected subset 3309 Equivalent Water Height (EWH) time series of the Level-2 GRACE and GRACE-FO gravity field processed by the CSR, GRAZ, GFZ and JPL centers simultaneously, after applying the DDK7 and Lobe-Edge filters and the first iteration of the M-SSA gap filling. Selected time series encompass a variety of signals of interest (see Figure S7 in Supporting Information S1 for a map of the chosen locations). The box plot shows the distribution of the normalized eigenvalues over the 3309 EWH time series. The dotted red line shows the variance reduction of the initial EWH time series given by the sum of Reconstructed Components (RCs). The red line highlights a drop in eigenvalues after rank 8, that is, the limit of eigenvectors we used for signal reconstruction.

while the rest of the time series remains identical for each processing center (Figure 4b and Figure S4 in Supporting Information S1 for additional examples).

3. Once outliers have been identified and replaced, we seek to improve the gap filling values, initially interpolated (by including third order polynomial, annual, and semiannual terms), in the observational gaps. Therefore, we perform a M-SSA in an iterative scheme for each of the resulting four EWH time series simultaneously, corresponding to the four processing centers, filtered of their outliers and evenly spaced by interpolation (including third order polynomial, annual, and semiannual terms). We use, once again, a sliding window of size $M = N/2$, half the length N of the GRACE/GRACE-FO period considered. M is chosen in order to capture the annual and long-term trends dominating the GRACE/GRACE-FO observations. To our knowledge, there is no optimal criterion to select M, but to provide separability of the series. Our value is chosen according to sensitivity tests summarized in Figure S6a in Supporting Information S1. Data gaps are then iteratively replaced, in all solutions, by the sum of the first N_c RCs resulting from the M-SSA on their combination. The value of N_c is chosen based on Figure 5, which shows the box plots of normalized eigenvalues obtained from M-SSA analyses for all four centers for a selected subset of 3309 EWH time series encompassing a variety of signals of interests (see Figure S7 in Supporting Information S1 for location of the chosen EWH). Eigenvalues rapidly decrease until a noticeable drop after rank 8, with the first 8 EOFs capturing 72.7% of the original EWH time series variance, motivating the choice of $N_c = 8$ (see also Figure S6b in Supporting Information S1 for additional tests on parameter N_c). Note that adding EWH time series of nearby points at the same latitude in the M-SSA gap filling procedure has only little impact on the reconstruction and is therefore not considered (Figure S6c in Supporting Information S1). Iterations are then performed until a convergence criterion, χ_c, between the reconstructed signal at iteration k, $\sigma_k^c(t, \lambda, \varphi)$, associated with

standard deviation $\varsigma\left(\sigma_k^c\right)$, and its previous iteration $k-1$ is reached. χ_c is defined, at iteration k, for n missing observations, $n \ll N$, as:

$$\chi_c(\lambda,\varphi) = \sqrt{\frac{\sum_{t=1}^{n}\left(\sigma_{k-1}^c(t,\lambda,\varphi) - \sigma_k^c(t,\lambda,\varphi)\right)^2}{\varsigma\left(\sigma_{k-1}^c\right)\cdot\varsigma\left(\sigma_k^c\right)}} \tag{2}$$

and satisfied for $\chi_c < 0.1$ or $n > 100$. Figure 4c shows an example, for a single processing center, of the successive signal reconstruction iterations until the convergence criterion, typically ranging between 7 and 16, is met (see Figure S4 in Supporting Information S1 for more examples).

The proposed gap filling method benefits from using solutions arising from four different processing centers by reconstructing observational gaps using only common signals retrieved by all solutions, thus limiting potential processing artifacts. In order to validate the method for filling the long 11-month gap between GRACE and GRACE-FO missions, we perform a synthetic test. Because modeling GRACE or GRACE-FO noise content is challenging due to its unknown exact structure, we artificially remove year 2008 of the GRACE dataset and test our gap filling method by reconstructing this missing year, in addition to existing missing dates. The reconstruction for year 2008 of an EWH time series located in the Caspian Sea is consistent with the original signal, with differences between the original and reconstructed signals of the order of differences between different GRACE solutions (Figure 4d). The reconstructed time series captures particularly well the strong annual variations over the Caspian Sea, as well as the regional trend of decreasing mass. However only signals based on the statistical content of the entire time series can be reconstructed, discarding unusual events (ex: heavy rainfall, earthquakes, etc.). Additional examples are provided in Figure S4 in Supporting Information S1, and effects of the M-SSA parameters on the reconstruction of year 2008 are assessed in Figures S5 and S6 in Supporting Information S1. Overall, the iterative M-SSA reconstruction proves more efficient at signal reconstruction than a linear or an ordinary least squares estimation-based interpolation (including third order polynomial, annual, and semiannual terms) interpolation (Figure S8 in Supporting Information S1), except for EWH time series of low amplitude signals, where performances are equivalent (Figure S4b in Supporting Information S1). Once gaps in the EWH time series have been satisfyingly filled to obtain evenly sampled time series, spatio-temporal filtering using M-SSA can be performed.

3.4. Spatio-Temporal Filtering With M-SSA

The second step of our method consists in performing a spatial filtering using the M-SSA to remove the remaining spatial noise. First, we average the four EWH time series obtained after gap filling, resulting from the four processing centers, into a single time series. Indeed, since applying the MSSA independently on the four time series does not improve the final result (see Figure S9 in Supporting Information S1), averaging them makes the method computationally more rapid. Then, as we aim at removing residual spatially correlated noise, namely the spurious North-South stripes, we apply the M-SSA on the EWH time series at each point of the global $1° \times 1°$ grid and, simultaneously, at its 3 neighboring EWH time series in both east and west directions, at the same latitude, 2° apart from each other (Prevost et al., 2019). Thus, to filter a single EWH time series, seven EWH time series are used. The number, distribution and distance between the neighbors of the reconstructed time series are defined by the spatial wavelength and shape of the spatially uncorrelated North-South stripes in order to extract only the correlated geophysical signals from the EWH time series through the M-SSA analysis. Parameters of the M-SSA for the spatial filtering step include a window size of $M = 13$ and a number of components for the reconstruction of $N_c = 8$. Note that M for M-SSA filtering is significantly smaller than for gap filling since we are now more interested in retaining high frequency variations in the gravity fields rather than capturing its main features for reconstruction. Sensitivity tests on M-SSA filtering parameters M, N_c, number and distance of neighboring EWH time series are provided in Figure S10 in Supporting Information S1. Note that N_c is defined similarly to the M-SSA reconstruction method, but now based on the eigenvalues of the M-SSA analysis of a EWH time series and its neighboring time series (see Figure S11 in Supporting Information S1).

For example, Figure 6 shows the M-SSA decomposition of the CSR EWH time series obtained after gap filling, for a point located in the Caspian Sea. The first 8 RCs show the potential of the method to separate and retrieve the dominant long term variation of the Caspian Sea (RC1), strong annual (RC2, RC3, RC4) variations as well as

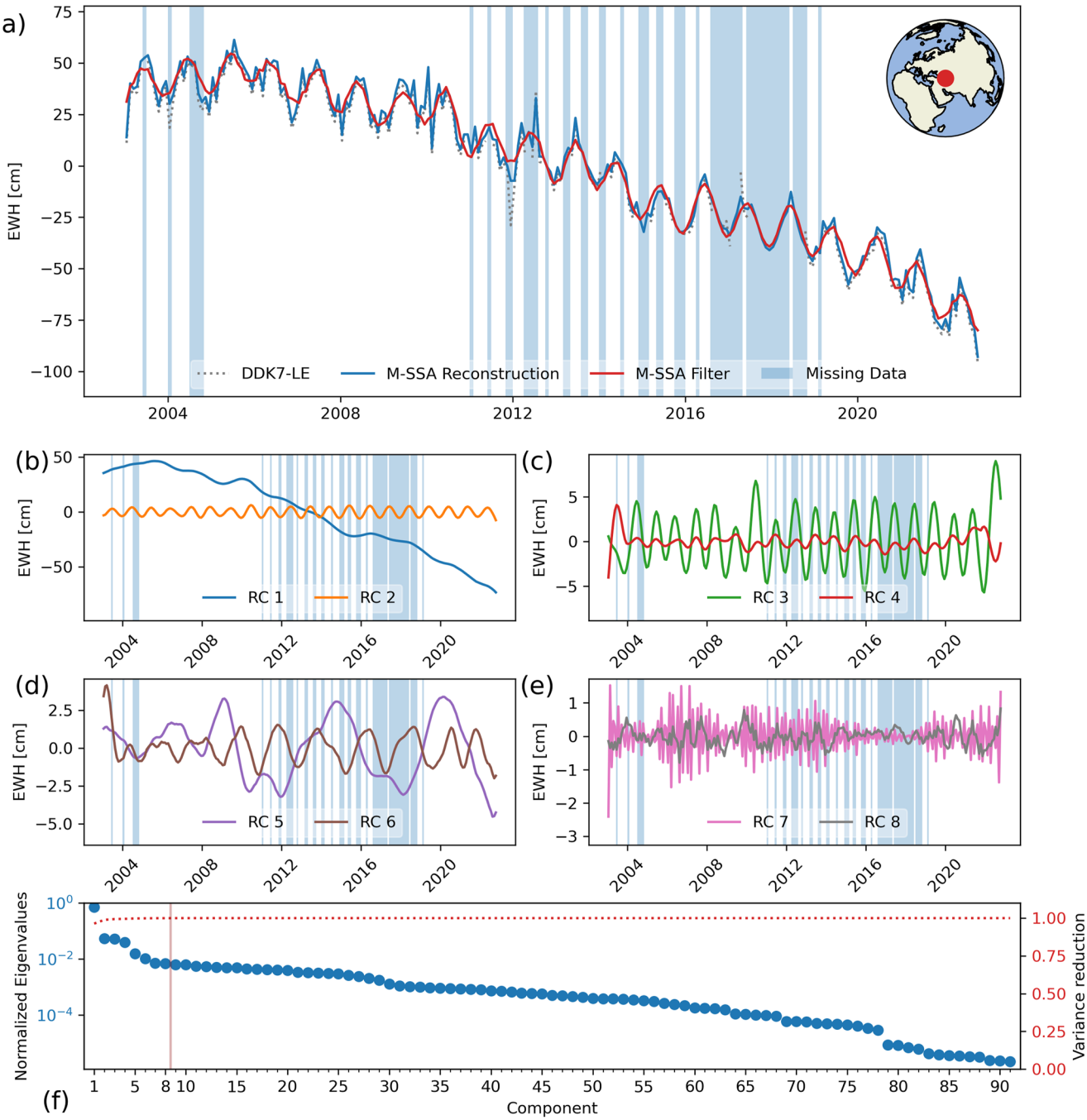

Figure 6. M-SSA spatio-temporal decomposition of the surface mass anomalies for a point located in the Caspian Sea (51°E, 41°N). Time series (a) shows the final EWH time series, after the DDK7 and Lobe-Edge filtering (LE filter, presented in Section 3.4, further reduces striping noise), M-SSA gap filling, using information from four processing centers, and spatial filtering, using an EWH time series and its neighbors located at the same latitude (red), compared to the gap filling procedure only (blue), and the initial DDK7-filtered (dotted gray) time series. (b–f) display the first 8 RCs of the decomposition, sorted by their corresponding eigenvalue. (g) Shows the normalized eigenvalues obtained from the M-SSA spatial filtering.

multi-annual variations (RC5, RC6). In fact, most of the variance of the filtered and evenly sampled EWH time series can be explained by the first 8 components (Figure 6f). The final EWH time series, after both the gap filling and spatial filtering steps, show that the complete method efficiently removes high frequency signal compared to the gap filling step and the initial DDK7-filtered time series (6a). The high frequency signal is unlikely related to changes in the Caspian sea level as supported by satellite altimetry measurements (J. Chen et al., 2017). Other examples of MSSA decomposition at various locations are provided in Figure S12 in Supporting Information S1.

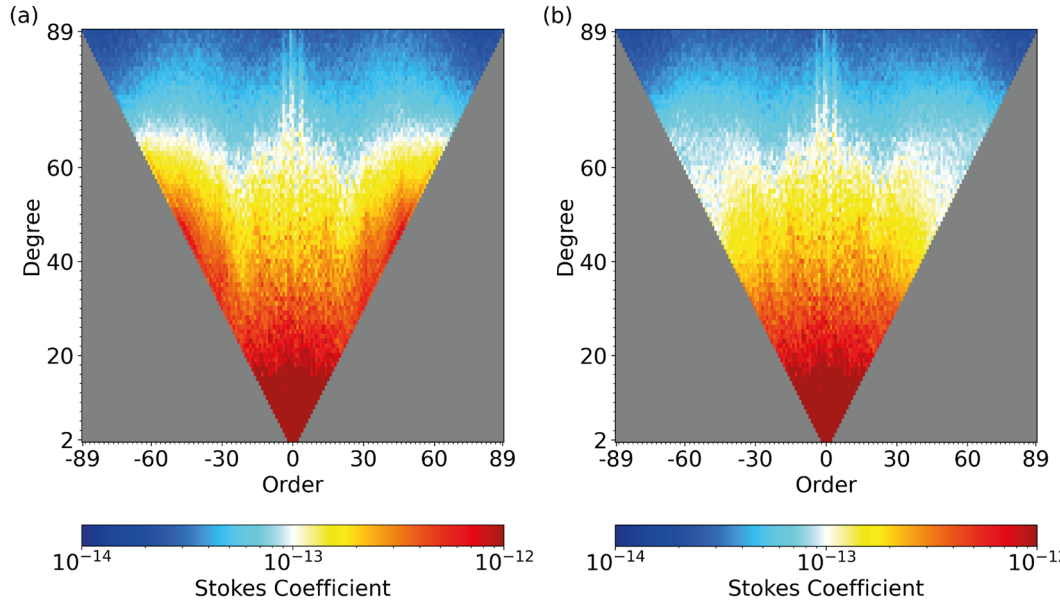

Figure 7. (a) Intensity spectrum of Stokes coefficients of the average of GRACE/GRACE-FO monthly surface mass anomaly, after DDK7 and M-SSA gap filling and spatial filtering, and once dominant geophysical signals have been removed using parametric functions. These signals include a degree-3 polynomial function, reflecting linear trends and multi-annual signals. Dominant seasonal signals are accounted for by removing from each monthly solution, its monthly averaged over the observational period. (b) Intensity spectrum of (a) after applying the Lobe-Edge filter on it for $\alpha = 1.5$.

3.5. Complementary Filtering in the Spherical Harmonics Domain: Lobe-Edge Filter

As mentioned at the end of Section 2.2, in order to refine an initial GRACE/GRACE-FO M-SSA solution, based on DDK7 filtering, we have designed an additional filter, named LE, to be applied after the decorrelation filter and before the M-SSA gap filling and filtering procedures to further reduce North-South stripes. To build this filter, we investigated the noise content of our initial GRACE/GRACE-FO M-SSA solution by looking at the average GRACE/GRACE-FO surface mass anomalies, after an initial DDK7 filtering, M-SSA gap filling and spatial filtering, and once dominant geophysical signals have been removed using parametric functions. A degree-3 polynomial function, representing linear trends and multi-annual signals, is removed while dominant seasonal signals are subtracted by their monthly averages throughout the observational period from each monthly solution, capturing the largest part of expected geophysical signals (Figure S13 in Supporting Information S1). Residuals between the gravity fields and the parametric functions are expressed in terms of Stokes coefficients $Y^r_{l,m}$, which is the mean value of $C^r_{l,m}$ and $S^r_{l,m}$, for a given degree l and order m. One can see that for $l > 25$, the amplitude of SH sectoral or close to sectoral (l close to abs(m)) is amplified compared to the amplitude of zonal or tesseral harmonics (Figure 7a). We thus define the LE filter, for which each coefficient, $F^{LE}_{l,m}$, for a given exponent α is:

$$\begin{cases} F^{LE}_{l,m} = \left(\dfrac{\frac{1}{6} \cdot \sum_{n=-1}^{1} \mathrm{abs}\left(Y^r_{l-n,m-n} + Y^r_{l-n,n-m} \right)}{\frac{1}{41} \cdot \sum_{n=-20}^{20} Y^r_{l,n}} \right)^{\alpha} & \text{for} \quad F_{l,m} \geq 1, \quad l \geq 25, \quad m \geq 25 \\ F^{LE}_{l,m} = 1 & \text{otherwise.} \end{cases} \tag{3}$$

By averaging the residual signal $Y^r_{l,m}$, for $l \geq 25$, m ≥ 25 and dividing its amplitude by the mean amplitude of $Y^r_{l,m}$, $-20 \leq m \leq 20$, we design a filter that is adapted to dampen the amplitude of the lobes of residual signal detected. The value of exponent α, here equal to 1.5, is chosen to ensure that the signal amplitude in the lobes for a given degree l, after LE filter has been applied, is comparable to its value over all orders m. Outside of the lobes, no additional filtering is performed. Coefficients of the LE filter are shown on Figure S2 in Supporting Information S1 (see Figure S14 in Supporting Information S1 for LE filters coefficients for various values of *alpha*) and its effect on residual data on Figure 7b. By design, coefficients of order $-20 \leq m \leq 20$ are not impacted by LE

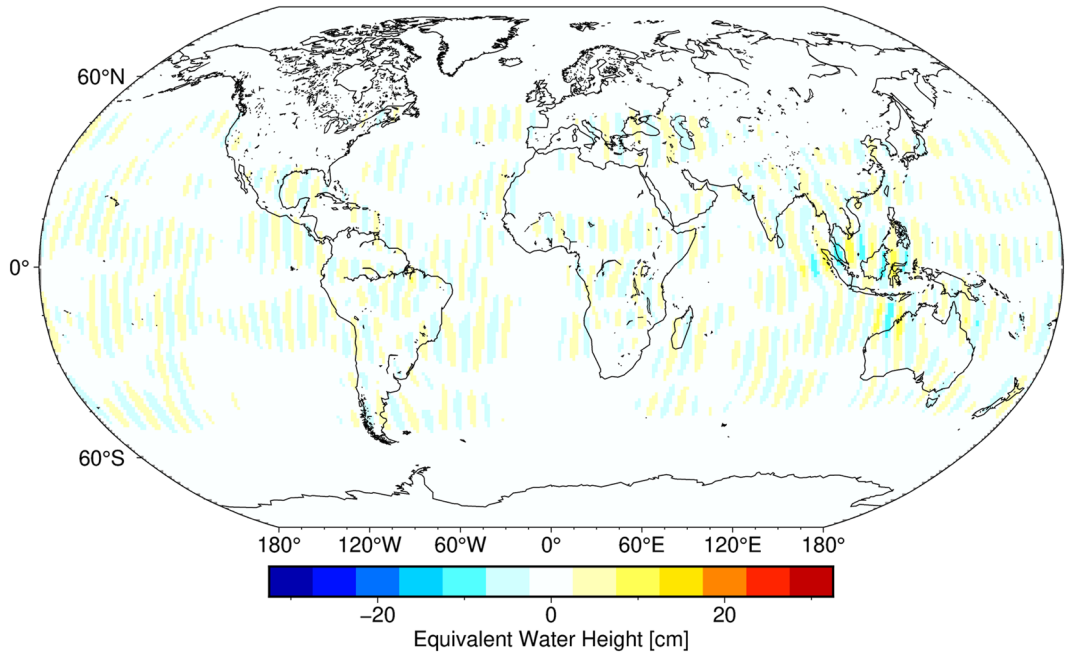

Figure 8. Map of the differences between the combined DDK7 + Lobe-Edge, with filter exponent $\alpha = 1.5$, and DDK7 only filtered GRACE-FO July 2019 monthly solutions, expressed in Equivalent Water Height.

filtering, whereas coefficients of degrees $l = 40$ to 50 and orders $m \geq 25$ can reach values up to 5 to efficiently filter persistent non-physical noise detected by our approach.

The LE filter is applied to monthly GRACE and GRACE-FO solutions $Y_{l,m}$, after DDK7 filtering, as:

$$Y_{l,m}^{LE} = \frac{Y_{l,m}}{F_{l,m}^{LE}} \tag{4}$$

Figure 8 shows an example of the impact of applying the additional LE filter to the DDK7-filtered GRACE-FO July 2019 monthly solution in the spatial domain. LE filtering efficiently removes spurious North-South stripes with significant amplitude, reaching up to ∼10 cm. In fact, the amplitude of North-South stripes removal is determined by the choice of LE filter exponent parameter α and lies in a compromise between efficiently filtering noise and preserving signals of geophysical origin. In particular, we notice that the stripes amplitude is higher in the region affected by the 2004 Mw 9.1 Sumatra-Andaman earthquake (Figure 8). This illustrates the fact that while the LE filter dampens the noise, it also dampens some physical signal. However, the gain in removing noise is larger than the loss of signal improving the global signal to noise ratio. Examples of results for other values of α are provided in Figure S15 in Supporting Information S1 for July 2019, and a particular attention is given to the 2004 Mw 9.1 Sumatra-Adaman earthquake region (Figure S16 in Supporting Information S1). The impact of applying LE filter can also be evaluated on EWH time series, where it helps removing high amplitude spikes that are unlikely to have a geophysical origin (Figure 9).

Overall, the LE filter proves efficient at removing residual North-South striping noise, after DDK filtering (Figure 8). We therefore include the LE filter in our GRACE/GRACE-FO post-processing strategy, after applying DDK7 and prior to perform M-SSA gap filling and filtering procedures. Examples of the full M-SSA spatio-temporal decomposition, after DDK7, with or without LE filtering, M-SSA gap filling and spatial filtering, are provided in Figures S12 and S17 in Supporting Information S1 respectively. Our final GRACE/GRACE-FO M-SSA solution, for which results are presented and discussed in following, is therefore a combination of DDK7 and LE filtering, with M-SSA gap filling and local filtering.

3.6. Results

We compare our final GRACE/GRACE-FO M-SSA solution with two other solutions in SH, all corrected for GIA contributions using the ICE-6G-D model (Argus et al., 2014; Peltier et al., 2015, 2018). The first one is

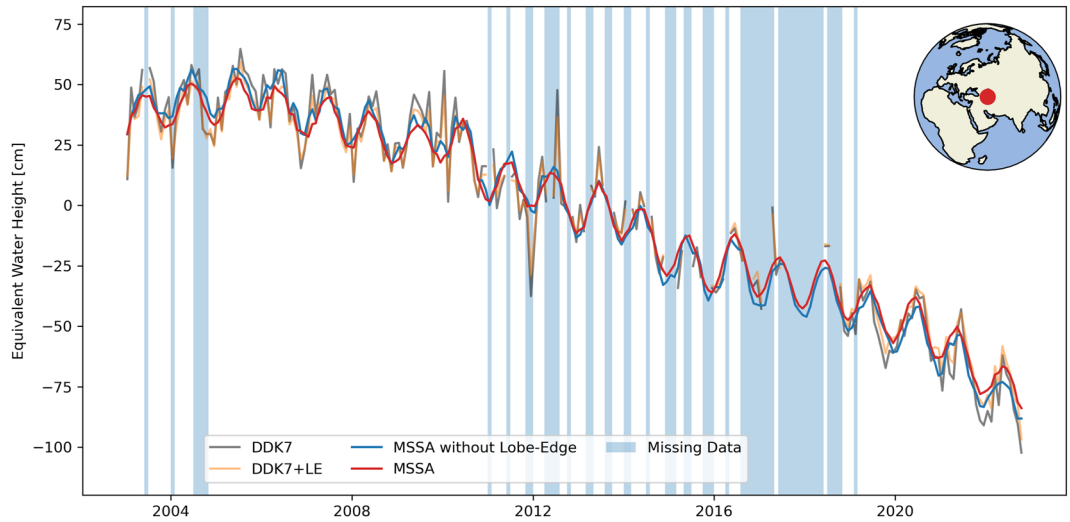

Figure 9. Comparison of GRACE/GRACE-FO Equivalent Water Height time series after DDK7 filtering (gray), DDK7 and Lobe-Edge filtering (orange), DDK7 filtering, M-SSA gap filling and spatial filtering (blue) or DDK7 and LE filtering, M-SSA gap filling and spatial filtering (red) for a point located in the Caspian Sea (51°E, 41°N).

the average of SH solutions processed by CSR, GRAZ, GFZ and JPL, filtered using DDK5, which is commonly used for geophysical applications (e.g., Sakumura et al., 2014). The second one uses DDK7, which is the initial filtering of the GRACE and GRACE-FO gravity fields before LE filtering, M-SSA gap filling and filtering procedures developed in this study. Figure 10 shows maps of the GRACE EWH for the month of July 2007, relative to January 2007, for all three solutions, after removing the linear trend estimated over the 2003–2022 period. Differences between gravity fields, which highlight the noise content of solutions, proves the efficiency of the method proposed in this study to remove characteristic nonphysical North-South striping patterns in the GRACE gravity fields. While both the DDK5 (Figure 10a) and DDK7 (Figure 10b) filtered 2007 GRACE July–January solutions display persisting stripes, particularly visible in the oceans, the final M-SSA solution (Figure 10c) shows only negligible striping patterns. Note that this is also true without applying LE filtering, but with a higher noise level (Figure S18 in Supporting Information S1). Moreover, compared with a commonly used solution for geophysical applications (Figure 10a), the final M-SSA solution (Figure 10c) is initially filtered using DDK7 rather than DDK5, which further attenuates signals and smears them out over larger regions. While a simple DDK7 filtering of the gravity fields may retain smaller spatial wavelengths signals, the high noise content of the resulting solutions prevents geophysical interpretations (Figure 10b). Since the final GRACE/GRACE-FO-MSSA is initially filtered using DDK7, in combination with an objective filtering approach through M-SSA, it successfully retains a higher spatial resolution than DDK5-filtered solutions, while removing sufficient North-South stripes to allow for geophysical interpretation. For example, the gravity signature of seasonal variations in surface and groundwater in the Mississippi river basin in Central United States (J. Chen et al., 2007; Rodell et al., 2007; Larochelle et al., 2022) appears spatially more focused in the GRACE/GRACE-FO-M-SSA solution than in the DDK5 averaged solution, and is undetectable in the DDK7 averaged solution.

Figure 11a shows the mean trend of surface mass anomaly of the final GRACE M-SSA solution, from January 2003 to December 2021. While the noise content of the GRACE M-SSA trend solution reaches a level comparable to the trend of the average of CSR, GFZ, GRAZ and JPL solutions filtered by DDK5, its spatial resolution, and therefore signal attenuation, is comparable to the DDK7-filtered one (Figure S19 in Supporting Information S1). Indeed, while major large scale long-term evolving phenomena, such as recent ice-sheets melting (ex: Greenland) or large variations in continental hydrology (ex: Caspian sea), are seen in all solutions, smaller spatial scales features consistent with regional geophysical processes are visible in the GRACE M-SSA solution including smaller magnitude earthquakes (ex: 2009 Mw 8.0 Samoa outer-rise earthquake) or smaller glaciers ice mass loss (ex: South Georgia; Prevost et al., 2019). Consequently, long-term trends between the commonly used average of CSR, GFZ, GRAZ and JPL solutions filtered by DDK5 and the GRACE M-SSA solution may locally differ. For example, Figure 11b shows comparisons of EWH time series for all solutions at a selected set of locations (see Figure S20 in Supporting Information S1 for differences with respect to our solution). While trends may

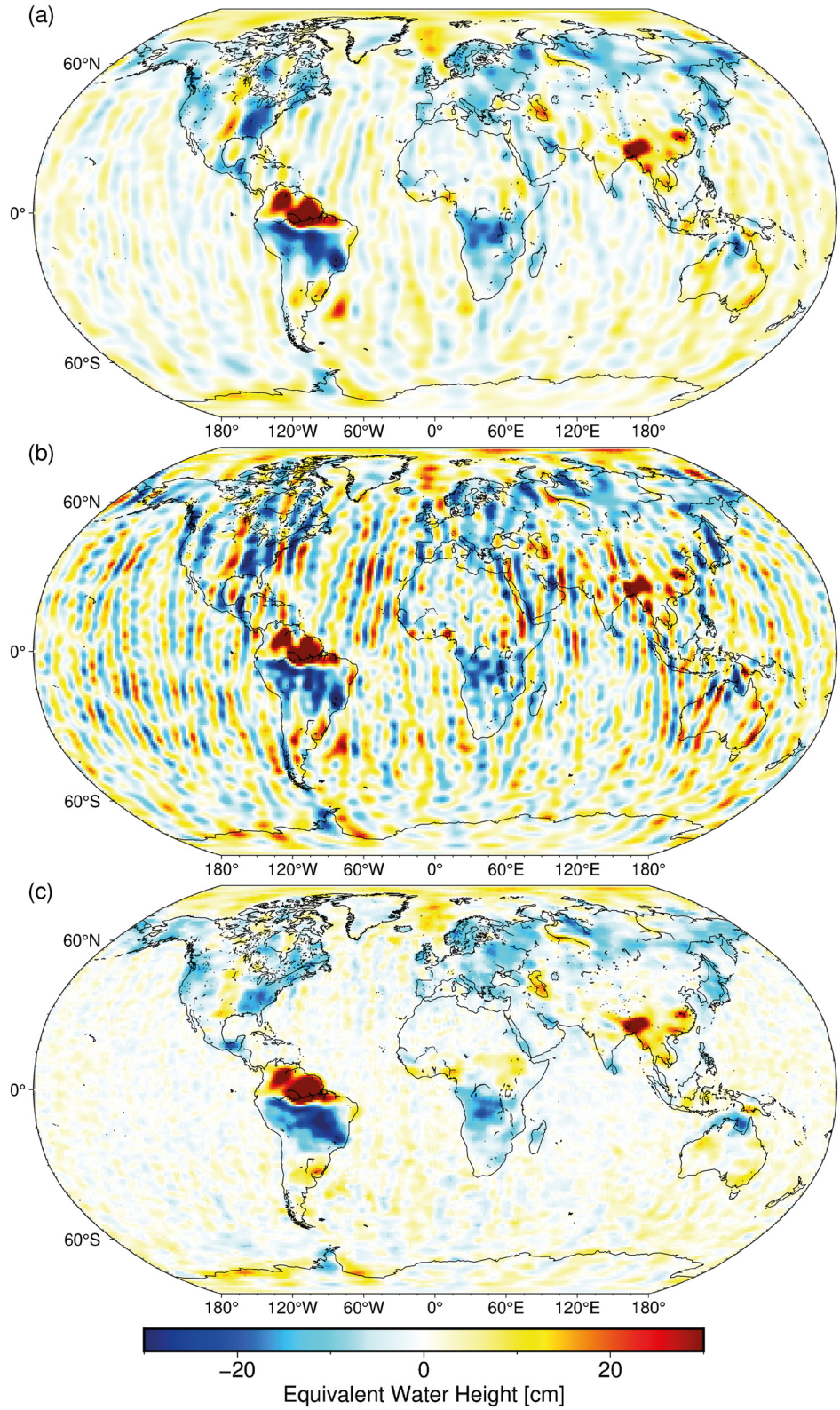

Figure 10. GRACE surface mass anomaly for the month of July 2007, relative to January 2007, expressed in Equivalent Water Height, corrected for Glacial Isostatic Adjustment contributions (ICE-6G-D, Peltier et al., 2018) for the average of CSR, GFZ, GRAZ and JPL solutions after applying (a) DDK5 filter, (b) DDK7 filter, and (c) the final GRACE M-SSA solution presented in this study.

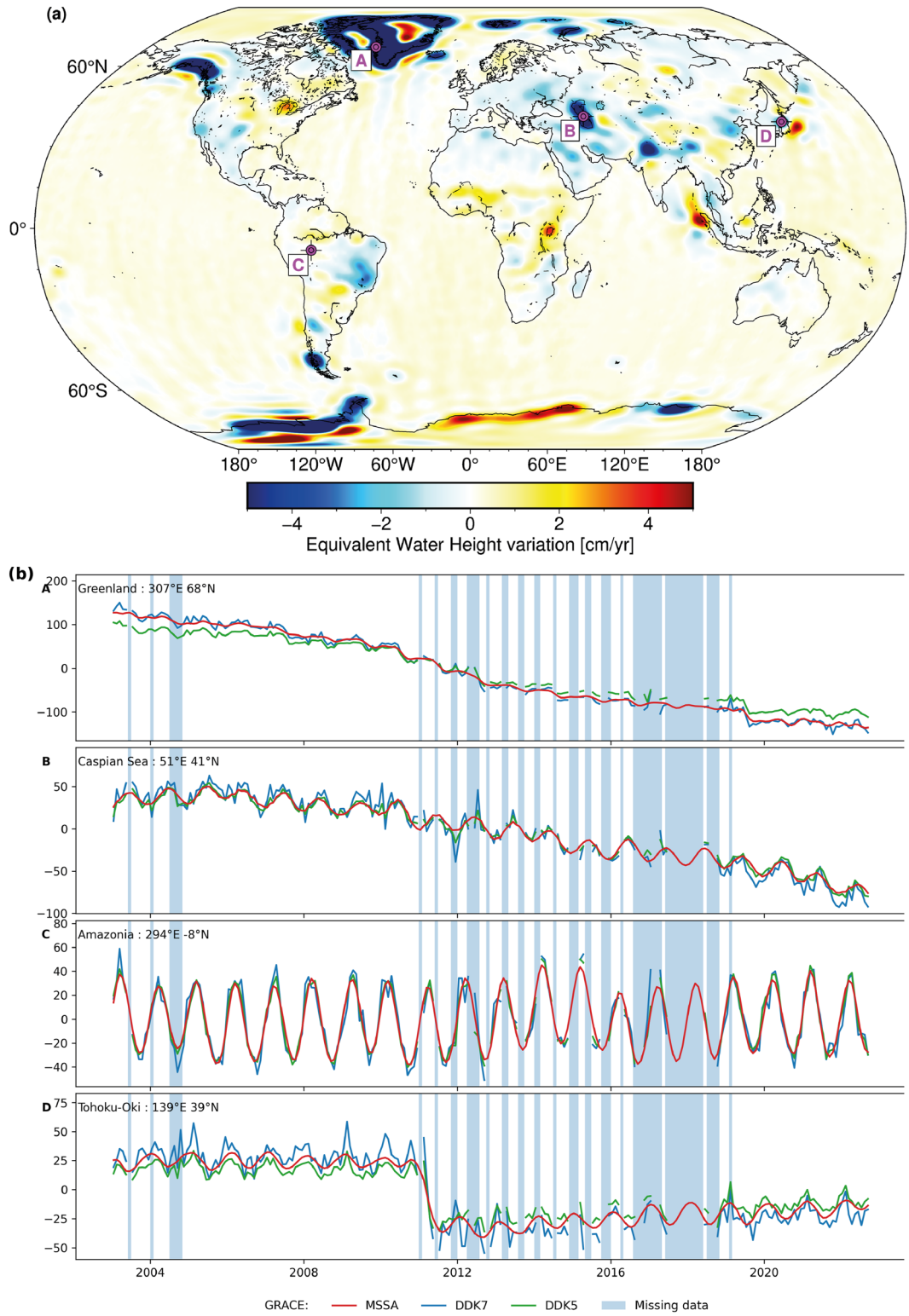

Figure 11. (a) Mean rate of surface mass anomaly of the final GRACE/GRACE-FO M-SSA solution presented in this study, from January 2003 to December 2021, expressed in Equivalent Water Height (EWH) per year. (b) Comparisons of EWH time series at points located in Greenland, the Caspian sea, the Amazonian basin and in the region of the 2011 Mw 9.1 Tohoku-Oki earthquake, pointed out on (a). EWH are shown for the average of CSR, GFZ, GRAZ and JPL solutions after applying DDK5 filter (green), DDK7 filter (blue), and the final GRACE/GRACE-FO M-SSA solution presented in this study (red).

agree in hydrological basins where mass variations occur at large scale such as the Amazonian basin, they tend to disagree in regions with more heterogeneity including for example, Greenland coastal area and the Caspian sea, potentially leading to an improvement in regional mass balance such as in Greenland using solutions with a higher spatial resolution. Nevertheless, the GRACE M-SSA solution does not retrieve abrupt mass change related for example, to the co-seismic gravity signal of the 2011 Mw 9.1 Tohoku-Oki earthquake, as well as the average of CSR, GFZ, GRAZ and JPL solutions filtered by DDK7. This is due to temporal filtering associated with the M-SSA method. A specific processing over regions affected by large earthquakes would be required to improve the final GRACE-M-SSA solution but is beyond the scope of this study.

Overall, the GRACE/GRACE-FO M-SSA solution, including DDK7, LE filtering, M-SSA gap filling and spatio-temporal filtering, efficiently removes characteristic North-South striping pattern, while retaining a higher spatial resolution than the widely used average of gravity fields SH solutions filtered by DDK5. Main features in trend and annual variability of the final GRACE/GRACE-FO M-SSA time series are comparable to those of DDK7 filtered gravity fields, consistent with the rest of the time series over reconstructed missing observations, and show a significantly lower noise content.

4. Discussion

We now focus on verifying consistency between our final GRACE/GRACE-FO M-SSA solution and independent datasets, including observations, models and different GRACE/GRACE-FO processing strategies, to assess the quality of both gap filling and spatio-temporal filtering at the global and local scale using the method developed in this study.

4.1. Global Scale Comparisons

4.1.1. Gap Filling Validation for Low Spherical Harmonics Gravity Field Coefficients: Comparison With SLR and Swarm Data

We seek to compare the final GRACE M-SSA solution with independent observation of low SH degrees, or long wavelengths signals, of the Earth's gravity field, namely with SLR observations and data from the Swarm mission.

SLR orbits are determined through the measure of the round trip time of a laser beam between satellites and ground tracking stations. Due to their spherical geometry and favorable area-to-mass ratio limiting a number of sources of uncertainties, SLR satellites are optimal for deriving accurate information on the Earth's gravity field. However, due to the limited distribution of ground tracking stations, the orbital height and the general measurement principle, SLR only gives access to temporal variations of the low SH degrees of the gravity field (Sośnica et al., 2015). Thus, here we compare the final GRACE/GRACE-FO M-SSA solution with the SLR Stokes coefficients of the gravity field provided by CSR up to the degree 6 order 1 (excepted the degree 6 order 0) (Cheng et al., 2011). As a reminder, we have replaced the $C_{2,0}$ and $C_{3,0}$ coefficients, starting in January 2003 and March 2012 respectively, according to the Technical Note 14 (TN-14; J. Chen et al., 2005; Loomis et al., 2020). Root Mean Square Deviation (RMSD) of the difference between low degree Stokes coefficients of the GRACE/GRACE-FO M-SSA solution and CSR SLR estimates are negligible except for $C_{3,0}$ and $C_{5,0}$ over the January 2003–February 2012 period (Figure 12a). We attribute the abnormal high amplitude of $C_{3,0}$ prior to February 2012 to its replacement recommendation only after March 2012, likely due to considerable improvements in SLR derived $C_{3,0}$ related to the launch of the LAser RElativity Satellite mission. Established anti-correlated resonance between $C_{3,0}$ and $C_{5,0}$ may explain the large discrepancies between the GRACE M-SSA and SLR solutions for $C_{5,0}$ before March 2012 (Loomis et al., 2020; Sośnica et al., 2015). As a result, the annual mean amplitude of the RMSD between GRACE/GRACE-FO M-SSA and SLR Stokes coefficients (Figure 12b) decreases after March 2012 and more interestingly, remains at similar level during observational gaps filled by the method proposed in this study. This suggests that observational gaps filled by M-SSA are comparable to independent SLR observations for low degree Stokes coefficients. Existing GRACE and GRACE-FO observations for low degree Stokes coefficients, which are unlikely impacted by our post-processing filtering approach, remain consistent with SLR observations throughout the entire time series.

Alternatively, the Swarm mission launched in November 2013 by the European Space Agency, and designed for exploring the Earth Magnetic Field, also constitutes an opportunity to compare GRACE/GRACE-FO M-SSA

Figure 12. Time dependent Root Mean Square Deviation of the difference between low degree Stokes coefficients of the GRACE/GRACE-FO M-SSA solution and (a) CSR SLR estimates and (b) Swarm, and a time series of their cumulative variation over the 2003–2022 period (right). Coefficients $C_{2,0}$ and $C_{3,0}$ have been replaced according to the Technical Note 14 (TN-14; J. Chen et al., 2005; Loomis et al., 2020), starting in January 2003 and March 2012 respectively. GRACE and GRACE-FO observational gaps, reconstructed using the M-SSA approach proposed in this study, are highlighted in blue.

solution with independent low-degree Stokes coefficients of the gravity field. Indeed, using non-gravitational force models and the trajectory of the three Swarm satellites in low earth polar orbit, it is possible to retrieve Stokes coefficients of the Earth gravity field up to SH degree 12 (Teixeira da Encarnação et al., 2016, 2020). In fact, the Swarm solution for the low-degree Earth gravity field has been initially validated using GRACE data (Teixeira da Encarnação et al., 2016). The RMSD between the GRACE/GRACE-FO M-SSA and Swarm Stokes coefficient up to degree 12 indicate that, a year after the launch of the Swarm mission, both datasets are and remain comparable. In particular, no significant difference is observed during GRACE/GRACE-FO original observational gaps reconstructed using the method described in this paper.

4.1.2. Comparison With Hydrological Model

We now want to assess performances of our final GRACE M-SSA solution gap filling method with an independent dataset of higher spatial resolution. Since a large portion of the gravity field variations recorded by GRACE/GRACE-FO signal are driven by continental hydrology (Syed et al., 2008), GRACE solutions are commonly compared to independent estimates of variations in land hydrology such as the Global Land Data Assimilation System (GLDAS; Longuevergne et al., 2013). GLDAS provides estimates of land surface hydrology based on satellite and in-situ observations, combined with advanced land surface modeling and data assimilation techniques (Rodell et al., 2004). In particular, GLDAS provides $1° \times 1°$ grids of estimated variations in snow, canopy water and soil water components between the surface and 2 m depth but not deeper groundwater. We convert the GLDAS datasets into EWH, sum, and compare to the final GRACE/GRACE-FO M-SSA solution. Note that the GRACE/GRACE-FO M-SSA solution has been corrected for GIA contributions using the ICE6-G-D model Peltier et al. (2018) for comparison with GLDAS, which is not sensitive to GIA.

Significant discrepancies in RMSD between GRACE/GRACE-FO M-SSA and GLDAS averaged over continental areas, reaching up to 10 cm of EWH on global continental average, occur during the summer months, likely due to the absence of groundwater and ice components in GLDAS that bear large seasonal variations (Figure 13). Reconstructed months, through the M-SSA gap filling procedure, tend to reflect this feature, particularly during the 11-month gap between missions. Note that during this period, and toward the erratic end of the GRACE mission, GRACE/GRACE-FO M-SSA reconstructions also show large discrepancies with GLDAS from January to April, which are not annually recurrent, but do reach similar values in 2010 and 2011. In fact, the yearly RMSD between the final GRACE/GRACE-FO M-SSA solution and GLDAS, averaged over continental areas shows comparable values over the entire 2003–2022 time series, including M-SSA filled GRACE observational missing periods. While we do not argue that statistically reconstructed GRACE observations over missing months should be geophysically interpreted without caution, the final GRACE/GRACE-FO solution offers a continuous record of gravity field variations, that can help, for example, recovering the long-term evolution of some processes (earthquake cycle, GIA, recent ice melting, water depletion, etc.).

The gap filling procedure used to process the GRACE/GRACE-FO M-SSA is consistent, to first order, with independent observations including low degree Stokes coefficients derived from SLR and estimations of variations in land hydrology. We now seek to compare the quality of the GRACE/GRACE-FO M-SSA with other GRACE/GRACE-FO solutions to assess the potential of our final solution to efficiently remove North-South stripes while retaining smaller spatial wavelength geophysical signals.

4.1.3. Comparison With Other GRACE/GRACE-FO Solutions

A metric commonly used to quantify noise level in GRACE and GRACE-FO solutions is to compute the Root-Mean-Square Deviation (RMSD) value over the ocean (Bonin et al., 2012; Meyer et al., 2016). Since gravity fields have initially been corrected for non-tidal high-frequency atmospheric and oceanic mass variation models (AOD1B; Dobslaw et al., 2017) by the processing centers, signal over the ocean should be small, and dominated by remaining random errors. To further reduce any signal of geophysical origin, we first fit and remove a degree-3 polynomial, annual and semi-annual sine functions to EWH time series at each point of a global $1° \times 1°$ grid. This functions account for potential geophysical signals in the GRACE and GRACE-FO over the oceans, including leakage signals in coastal areas related to continental mass smeared out over large regions due to the missions' intrinsic spatial resolution and filtering approach. Note that we exclude regions of major earthquakes, by removing oceanic areas of observations around epicenters which size is determined based on the GRACE/GRACE-FO M-SSA mean rate of surface density anomaly. Earthquakes considered are the 2004 Mw 8.8 Sumatra-Andaman, 2010 Mw 9.1 Maule and 2011 Mw 9.1 Tohoku-Oki earthquakes. Finally, we exclude latitudes above $-45°$ and

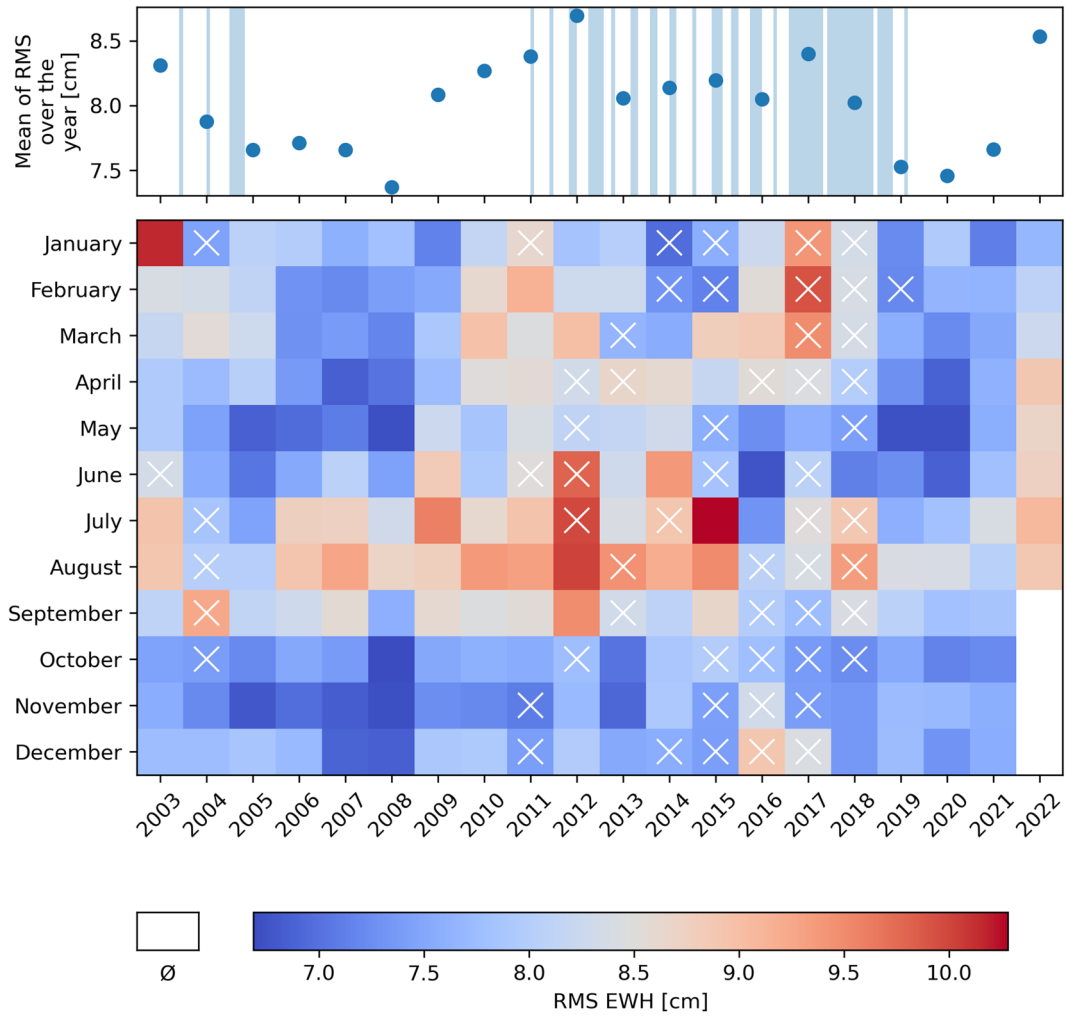

Figure 13. Root Mean Square Deviation (RMSD) over continental areas between the final GRACE/GRACE-FO M-SSA solution and the Global Land Data Assimilation System (Rodell et al., 2004), expressed in Equivalent Water Height. Yearly averaged RMSD (top) and monthly RMSD (bottom) are shown over the 2003–2022 period. Missing periods of GRACE/GRACE-FO observations, reconstructed using the M-SSA procedure proposed in this study are highlighted in light blue (top) and white crosses (bottom).

Table 1
Statistics of the Residual Signal Over the Ocean for Various Solutions Expressed in Equivalent Water Height (EWH) (cm)

Gravity Recovery And Climate Experiment (GRACE) solution	Mean EWH (cm)	Standard deviation EWH (cm)
GRACE M-SSA	0.30	0.069
GRACE M-SSA SH	0.67	0.239
GRACE DDK5	0.90	0.405
GRACE DDK7	2.08	0.951
GRACE COST-G DDK5	0.92	0.918
GRACE MASCONS CSR	0.36	0.056
GRACE MASCONS JPL	0.34	0.055

below 45°, to exclude regions where significant leakage of the continental ice-sheets and glaciers into the oceans occurs.

Figure S21 in Supporting Information S1 shows a map of the ocean region considered used to compute the RMSD. The noise level of the final GRACE/GRACE-FO M-SSA solution over the oceans remains low throughout the entire period considered (Figure 14a), with a mean EWH value of ~0.30 cm and a standard deviation of 0.069 cm (Table 1). To compare performances with other solutions, we also compute the difference of RMSD over the oceans between the final GRACE/GRACE-FO M-SSA solution and the average of DDK7-filtered SH CSR, GFZ, GRAZ and JPL solutions, the DDK5-filtered COST-G combination solution (Jäggi et al., 2020; Meyer et al., 2019), the CSR mascons independent processing strategy and the M-SSA SH (Figure S3 in Supporting Information S1; Prevost et al., 2019) (Figure 14). Absolute RMSD values over the oceans for all solutions are shown in Figure S22 in Supporting Information S1. The GRACE/GRACE-FO M-SSA solution efficiently removes noise compared

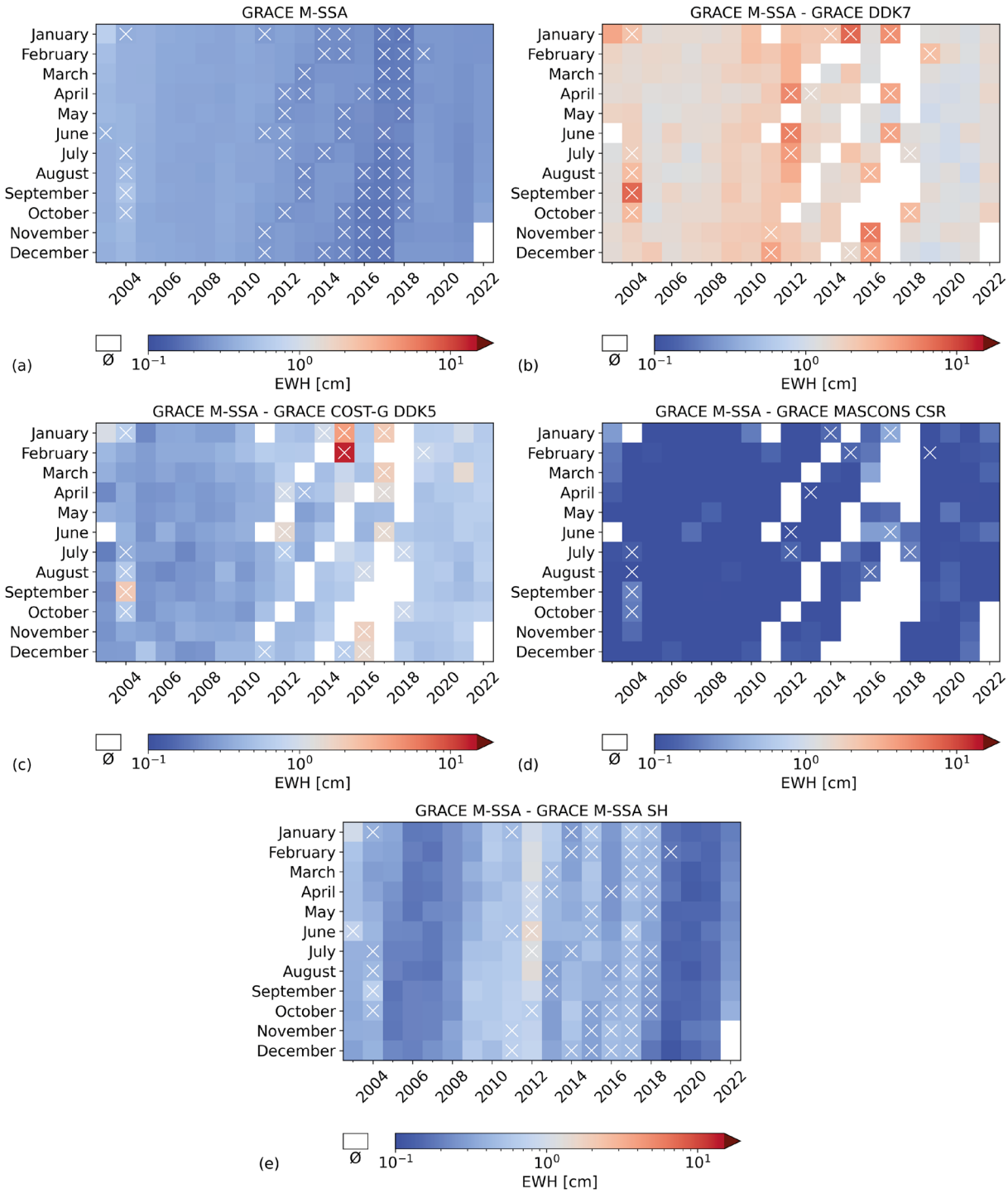

Figure 14. (a) Root-Mean-Square Deviation (RMSD) value of the final GRACE/GRACE-FO M-SSA solution over the ocean, expressed in terms of Equivalent Water Height (EWH), after fitting and removing a degree-3 polynomial, annual and semi-annual sine functions from EWH time series at each point of a global 1° × 1° grid. These functions account for potential signals of geophysical or leakage origin in the ocean. Regions of large earthquakes and latitudes below and above 45° are excluded from the RMSD computation (see Figure S21 in Supporting Information S1 for a map of the region considered). White crosses show the reconstructed periods using the M-SSA procedure. Difference of RMSD between the final GRACE/GRACE-FO M-SSA solution and (b) the average of DDK7-filtered CSR, GFZ, GRAZ and JPL solutions, (c) the DDK5-filtered COST-G combination solution, (d) the CSR mascons independent processing strategy and (e) the M-SSA SH solution from Prevost et al. (2019).

to DDK7-filtered solutions, which are the starting point of the method (Figure 14b), and contains lower noise level than the combined COST-G even though it is filtered at a higher level, using DDK5 (Figure 14c). More importantly, the GRACE/GRACE-FO M-SSA solution noise level over the ocean reaches the CSR mascons noise level, which is low by construction due to strong regularization in oceans, but with no a priori constraints or regularization on the noise or signal distribution (Figure 14d). Comparison with the average of DDK5-filtered SH CSR, GFZ, GRAZ and JPL solutions and JPL mascons solution yield similar conclusions (Table 1 and Figure S23 in Supporting Information S1). Finally, improvements of the method proposed in this study compared to the one proposed by Prevost et al. (2019) show significant noise reduction over the oceans (Figure 14e and Table 1).

Overall, the M-SSA based gap filling and filtering methods lead to a final GRACE/GRACE-FO M-SSA solution that is consistent with independent datasets and contains a lower noise level than the other SH solutions presented here, independently of the choice of a DDK7 or DDK5 filter, reaching the level of mascons solutions (Table 1). However, any filtering of the GRACE/GRACE-FO gravity fields generated from SH Stokes coefficients necessarily causes signal attenuation and leakage. Thus, at the local and regional scales, we compare the final GRACE/GRACE-FO solution, as well as other SH solutions, with the independent mascons processing technique.

4.2. Local and Regional Scale Comparisons

4.2.1. Comparisons of Equivalent Water Height Time Series

We compare EWH time series at a selected set of locations in regions of geophysical interest (Figure 15, difference with respect to our solution are presented in Figure S24 in Supporting Information S1). On one hand, the overall features retrieved with the GRACE/GRACE-FO M-SSA solution agree with all SH solutions, despite discrepancies in the higher frequency content of the time series, likely due to the noise content of each solution. In particular, the method proposed in this study agrees well with the initial method proposed by Prevost et al. (2019), with a larger portion of the North-South stripes removed thanks to the LE filter, and a simplified processing with M-SSA applied on EWH only. On the other hand, major differences between SH solutions and the CSR mascons solution appear. First, for a point located on the western central coast of Greenland (Figure 15a), the rate of surface mass loss is surprisingly twice larger for the CSR mascons solution than for SH solutions, all corrected for GIA contribution, in a region that is not covered by ice and thus where no mass variation related to recent ice melting is expected. In fact, the CSR mascons solution appears to have an ocean/continent limit rather than a physical limit based on ice-sheet/glacier location (Figure S25 in Supporting Information S1). Furthermore, for a point located in the region of the 2011 Mw 9.1 Tohoku-Oki earthquake (Figure 15b), the co-seismic gravity signal is four times larger in the CSR mascons than in the SH solutions, driven by the parametrization of the regularization matrix used to develop the mascons solution (Save et al., 2012, 2016). Such differences raise the question of GRACE and GRACE-FO mass variations validation to ground truth independent measurements to quantitatively assess solutions performances. For points located in the Caspian sea and the Amazonian basin, where large long-term and/or seasonal signals are expected, all solutions are in a good agreement. However, even small discrepancies between solutions can lead to significant differences in hydrological mass balance over large areas. Validation of solutions against independent observations is thus essential to assess solution quality (J. Chen et al., 2017).

4.2.2. Method Validation Through Regional Hydrological Mass Balance

To assess performances of our final GRACE/GRACE-FO M-SSA solution, compared to others, we seek validation through comparison with independent information at the regional scale, with the example of hydrological mass balance over reservoir impoundments. However, validating GRACE/GRACE-FO SH solutions comes with two major challenges.

Firstly, finding independent measurements of mass variations comparable to GRACE/GRACE-FO is difficult. Indeed, GRACE/GRACE-FO measures large scale combined variations in surface and groundwater, as well as within the solid Earth. In some regions, with minimal solid Earth related gravity variations, dense networks of groundwater measurements and available estimates of surface water components (snow, canopy, soil moisture) from other sources, namely models of land surface hydrology (ex: GLDAS, Rodell et al., 2004), it has been possible to validate GRACE/GRACE-FO measurements (Feng et al., 2013; Scanlon et al., 2012). In addition, comparison with satellite altimetry, offers interesting opportunities to validate GRACE/GRACE-FO solutions. In

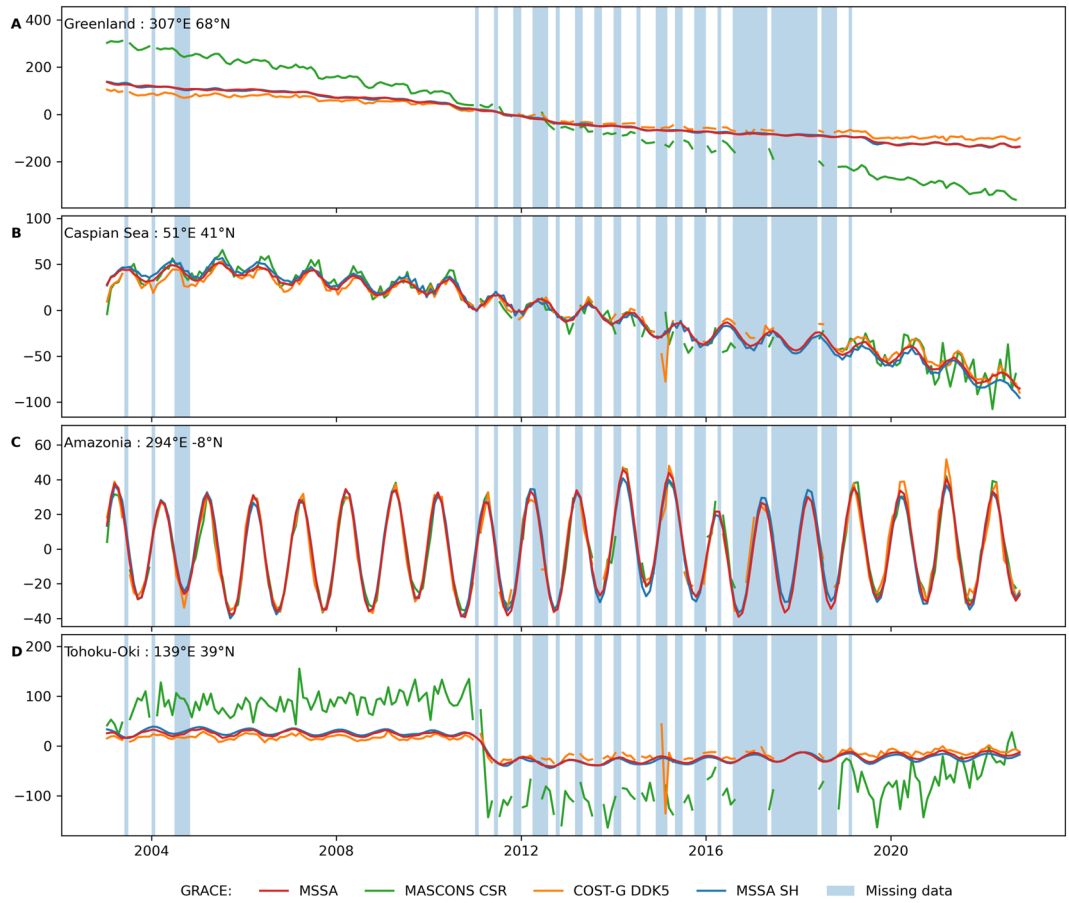

Figure 15. Time series of surface mass anomaly, expressed in cm of Equivalent Water Height (EWH), at points located in Greenland, in the Caspian sea, in the Amazonian basin and in the region of the 2011 Mw 9.1 Tohoku-Oki earthquake (see location map on Figure 11). EWH time series are compared for four different solutions: the final GRACE/GRACE-FO M-SSA solution presented in this study (red), the GRACE/GRACE-FO M-SSA solution based on Prevost et al. (2019) (blue), the combined COST-G solution after applying DDK5 (orange) and the CSR mascons solution (green).

particular, due to its large spatial extent, significant signal amplitude and minimal groundwater variations in the region, the Caspian sea has become an ideal candidate to seek validation of mass change measurements with sea level variations measured by satellite altimetry (Swenson & Wahr, 2007; J. Chen et al., 2017). Nonetheless, the comparison of GRACE/GRACE-FO SH estimates at the regional scale with independent datasets suffers another challenge.

Any filtering strategy of the GRACE/GRACE-FO solutions, on top of the missions intrinsic resolution, which is necessary to reduce North-South striping noise, causes spatial leakage error. This error is responsible for signal amplitude attenuation and causes geophysical signals to smear out over large regions. Reducing leakage bias is therefore essential to quantify mass variations at the regional scale, and requires independent sources of information. A commonly used method is the model-derived scaling factors, which model-dependency (Landerer & Swenson, 2012) can be overcome using data-driven methods (Dobslaw et al., 2020; Vishwakarma et al., 2017). Another well established method is forward modeling which uses a priori information on the source location to estimate the amplitude of the mass change through an iterative numerical scheme by minimizing differences of the truncated and filtered GRACE/GRACE-FO data and a priori model until an arbitrary threshold criterion is met (J. Chen et al., 2015; J. Chen, Wilson, Blankenship et al., 2006; J. Chen, Wilson, & Tapley, 2006). The latter method has been used for various geophysical applications, from changes in ice mass (Wouters et al., 2008), lake water storage (J. Chen et al., 2017) or ocean mass (Jeon et al., 2018).

Here, we develop a modified forward modeling approach and apply it to reservoir impoundments, for which the shape and maximum volume capacity are well known. We first apply both filters used in our GRACE/GRACE-FO

processing, namely DDK7 and LE, to the reservoir impoundment shape to obtain its theoretical filtered shape in the GRACE/GRACE-FO solution. We then perform, for each monthly gravity field, a linear regression between the DDK7+LE filtered GRACE/GRACE-FO observations and the filtered reservoir impoundment shape. The "true" reservoir impoundment volume variations are given by its actual surface times the time-dependent coefficient of the linear regression, and can be easily compared to its known capacity and date of commissioning.

In particular, we first consider the Boguchany Reservoir, impounded by a dam at Kodinsk, Russia, which is part of a major water storage system, including multiple dams on the Angara River, which flows out from Lake Baikal. The dam began to fill its reservoir in May 2012, with an expected maximum capacity of 58.2 km^3 of water (Jaguś et al., 2015). We also consider the Bakun embankment dam in Sarawak, Malaysia, on the Balui River (Oh et al., 2010, 2018), which started to be filled in late 2010, and reached its maximum capacity of 43.8 km^3 in 2011 (Tangdamrongsub et al., 2019). The Bakun dam has to be associated with the close by Murum reservoir, leading to non distinguishable signals at the GRACE/GRACE-FO spatial resolution. The Murum dam started to be filled in December 2014, up to its maximum capacity of 12.0 km^3. Figure 16 shows results of the method applied to several GRACE/GRACE-FO solutions for both reservoir impoundments. Particularly, we compared SH solutions using various filtering strategies, including the average of SH solutions processed by CSR, GRAZ, GFZ and JPL, filtered using DDK5, the M-SSA SH solution proposed by Prevost et al. (2019) and extended to GRACE-FO, and our final GRACE/GRACE-FO M-SSA solution. We also compare hydrological mass balance to CSR mascons solution, at its expected spatial resolution, and extending the mass balance over the same area used for SH solutions, that is, accounting for leakage. SH solutions detect large mass variations related to reservoir impoundments for both Boguchany and Bakun reservoirs and the maximum volumes retrieved for the GRACE/GRACE-FO solution, over observing periods only, are 56.31 and 37.02 km^3. These results agree best with the true maximum capacity of the reservoirs, down to the 5 km^3 level. Note that we estimate the Bakun maximum capacity from GRACE/GRACE-FO solutions prior to the Murum lake filling to isolate its contribution. Moreover, since it is possible to characterize exactly the effect of both the DDK and LE filters on attenuation and leakage of a known source, regional mass balance based on SH solutions are consistent with independent datasets once corrected for these effects. In contrast, volume retrieved by the CSR mascons solution at their expected spatial resolution are close to zero. When hydrological mass balance are performed over a larger area for CSR mascons, similar to the area used for SH solutions, we observe signals consistent with reservoir impoundments, but with a much lower amplitude than expected. This may be related to a significant regularization of the CSR mascons solution in a region with little mass variations, and unexpected anthropogenic activity, and unknown exact transfer function between a known source and its mascons description which could impact regional mass budgets.

5. Conclusions

In this article we develop a post-processing strategy for gap filling, combining and filtering pre-processed multiple GRACE/GRACE-FO Level-2 SH gravity field solutions, inspired by Prevost et al. (2019), with minimal a priori constraints on the signal or noise spatio-temporal evolution. First, we combine the DDK7 filter with a new LE filter, built to further reduce the remaining lobes of spurious errors, detected around SH degree 40. We then perform gap filling of missing observations in time series of EWH processed by four processing centers (CSR, GRAZ, GFZ, JPL), after identifying and removing outliers, and taking advantage of their common modes of variability using an iterative M-SSA. We then proceed to spatial filtering by applying the M-SSA on each averaged EWH time series, obtained from the four different solutions, and its near neighbors in the eastern and western directions to remove local striping artifacts.

We compare our final GRACE/GRACE-FO M-SSA solution with other solutions and seek ground truth through comparisons with independent observations. First, we ensure that gap filled periods, solely based on the iterative M-SSA scheme, are in agreement with low-degree Earth's gravity field derived from SLR, Swarm and GLDAS, a surface land hydrology model. Comparisons show the M-SSA method ability to satisfyingly reconstruct missing observations. Then, we investigate the noise content of the GRACE/GRACE-FO M-SSA solution over the oceans, which shows improvements compared to other SH solutions, and a level similar to mascons type solutions, that are regularized and/or constrained by construction. Finally, we show the potential of the method to retrieve short-wavelengths geophysical signals, often smeared out over large regions by highly filtered SH solutions or masked out by mascons solutions, using the example of hydrological mass balance of the Boguchany (Russia) and Bakun (Malaysia) reservoir impoundments. In turn, the GRACE/GRACE-FO M-SSA solution can reveal smaller

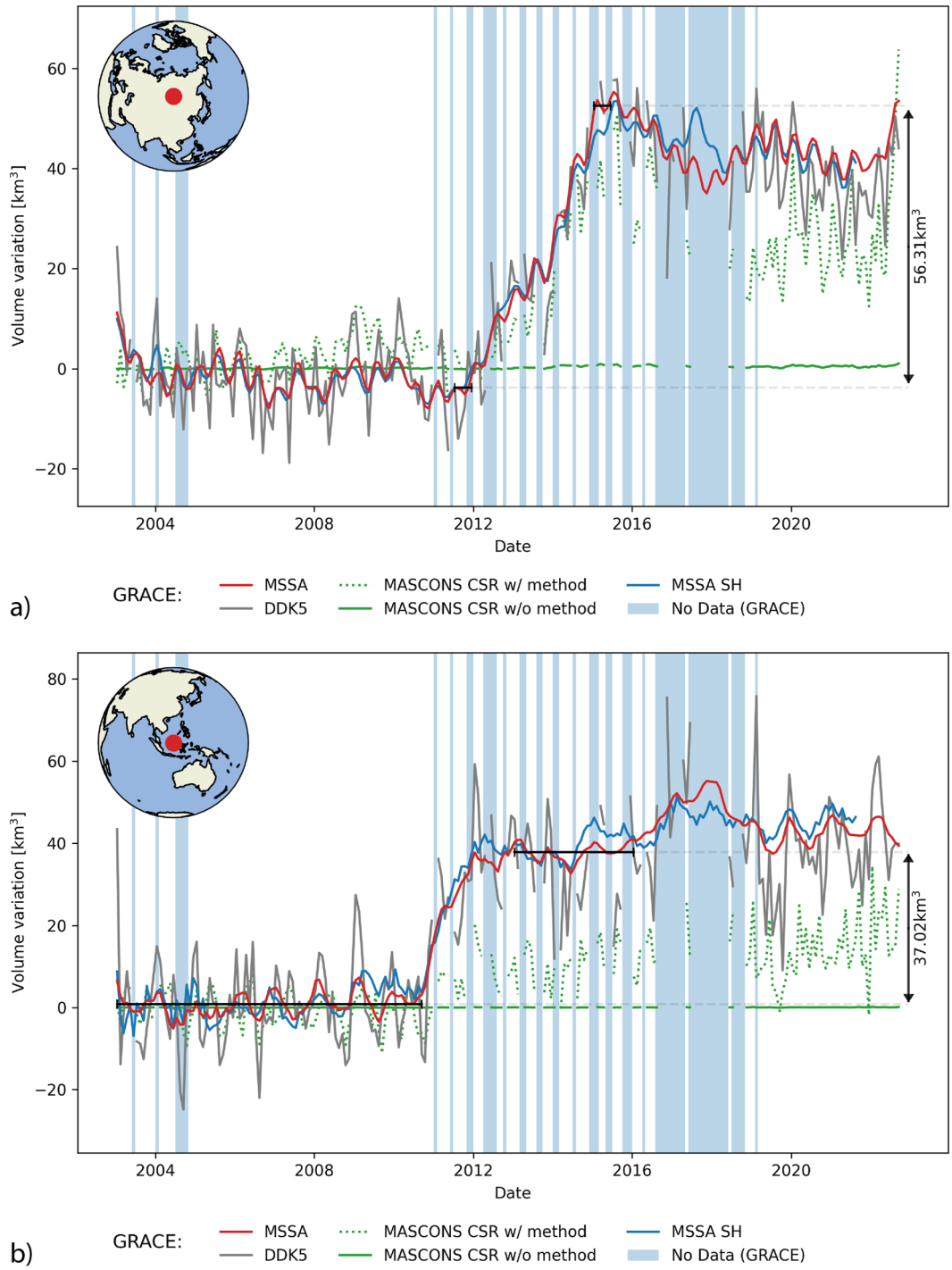

Figure 16. Volume variations of the (a) Boguchany Reservoir, impounded after the recent construction of a dam at Kodinsk, Russia, which is part of a major water storage system, including multiple dams on the Angara River, which flows out from Lake Baikal. The reservoir began to be filled in May 2012, with an expected maximum water capacity of 58.2 km^3 and (b) Bakun embankment dam in Sarawak, Malaysia, which started to be filled in late 2010, and maximum capacity of 43.8 km^3, associated with the close by Murum reservoir, which filling started in late 2014 for a maximum capacity of 12 km^3. Volume variations are computed using the modified forward model method proposed in this study, for the average of spherical harmonic solutions processed by CSR, GRAZ, GFZ and JPL, filtered using DDK5 (gray), the M-SSA SH solution proposed by Prevost et al. (2019) and extended to GRACE-FO (blue), and our final GRACE/GRACE-FO M-SSA solution (red). Estimates are compared to volume variations derived from the CSR mascons solution at its expected spatial resolution (solid green), and using a larger area accounting for leakage error (dashed green), based on the forward model proposed for SH solutions.

spatial scale signals, including gravity changes induced by smaller melting glaciers or smaller magnitudes earthquakes. The GRACE/GRACE-FO M-SSA solution is freely available through IPGP Research Collection (https://research-collection.ipgp.fr/) at the following DOI: https://doi.org/10.18715/IPGP.2023.lgquie56.

Data Availability Statement

Level-2 GRACE and GRACE-FO data used in this study are freely available and provided by the Center of Space Research (CSR) (https://dx.doi.org/10.5067/GRGSM-20C06 and https://dx.doi.org/10.5067/GFL20-MC060), the GeoForschungsZentrum (GFZ) (https://dx.doi.org/10.5880/GFZ.GRACE_06_GSM and https://dx.doi.org/10.5067/GFL20-MG060), the Institute of Geodesy of the University of Graz (GRAZ) (http://ftp.tugraz.at/outgoing/ITSG/GRACE/ITSG-Grace2018/monthly/monthly_n96/ and http://ftp.tugraz.at/outgoing/ITSG/GRACE/ITSG-Grace_operational/monthly/monthly_n96/) and the Jet Propulsion Laboratory (JPL) (https://dx.doi.org/10.5067/GRGSM-20J06 and https://dx.doi.org/10.5067/GFL20-MJ060). Stokes coefficient $C_{1,0}$ coefficients for GRACE and GRACE-FO are provided in the Technical Notes 13 (https://opendap.jpl.nasa.gov/opendap/allData/grace/docs/contents.html). Stokes coefficients $C_{3,0}$ and $C_{5,0}$ are available in Technical Note 14 (https://opendap.jpl.nasa.gov/opendap/allData/grace/docs/contents.html). GIA model used to compare with mascons and GLDAS model are provided by JPL https://opendap.jpl.nasa.gov/opendap/allData/tellus/L3/gia/1-deg/Tellus_GIA_L3_PELTIER_ICE6G-D_1-DEG_v1.0.nc. SLR data used for comparison are provided by CSR http://download.csr.utexas.edu/pub/slr/degree_5/CSR_Monthly_5x5_Gravity_Harmonics.txt and GLDAS is freely available at https://hydro1.gesdisc.eosdis.nasa.gov/data/GLDAS/GLDAS_NOAH10_M.2.1/GLDAS. Processing of the data has been done using `Python` (https://www.python.org/) using the M-SSA `pymssa` package (https://github.com/kieferk/pymssa) and `Python` interface for the Generic Mapping Tools `PyGMT` (https://www.pygmt.org/latest/). The final GRACE/GRACE-FO solution is freely available through IPGP Research Collection (https://research-collection.ipgp.fr/) at the following DOI: https://doi.org/10.18715/IPGP.2023.lgquie56.

Acknowledgments
We thank the two anonymous reviewers, as well as the editor and associate editor, for their useful comments and suggestions. This study was supported by the CNES-TOSCA HYDROGEODESY project.

References

Argus, D. F., Peltier, W. R., Drummond, R., & Moore, A. W. (2014). The Antarctica component of postglacial rebound model ice-6G_C (VM5a) based on GPS positioning, exposure age dating of ice thicknesses, and relative sea level histories. *Geophysical Journal International*, *198*(1), 537–563. https://doi.org/10.1093/gji/ggu140

Blazquez, A., Meyssignac, B., Lemoine, J., Berthier, E., Ribes, A., & Cazenave, A. (2018). Exploring the uncertainty in grace estimates of the mass redistributions at the Earth surface: Implications for the global water and sea level budgets. *Geophysical Journal International*, *215*(1), 415–430. https://doi.org/10.1093/gji/ggy293

Bonin, J. A., Bettadpur, S., & Tapley, B. D. (2012). High-frequency signal and noise estimates of CSR GRACE RL04. *Journal of Geodesy*, *86*(12), 1165–1177. https://doi.org/10.1007/s00190-012-0572-5

Bouih, M., Panet, I., Remy, D., Longuevergne, L., & Bonvalot, S. (2022). Deep mass redistribution prior to the 2010 Mw 8.8 Maule (Chile) earthquake revealed by GRACE satellite gravity. *Earth and Planetary Science Letters*, *584*, 117465. https://doi.org/10.1016/j.epsl.2022.117465

Cambiotti, G. (2020). Joint estimate of the coseismic 2011 Tohoku earthquake fault slip and post-seismic viscoelastic relaxation by GRACE data inversion. *Geophysical Journal International*, *220*(2), 1012–1022. https://doi.org/10.1093/gji/ggz485

Chambers, D. P. (2006). Observing seasonal steric sea level variations with grace and satellite altimetry. *Journal of Geophysical Research*, *111*(C3), C03010. https://doi.org/10.1029/2005jc002914

Chambers, D. P., & Willis, J. K. (2008). Analysis of large-scale ocean bottom pressure variability in the north Pacific. *Journal of Geophysical Research*, *113*(C11), C11003. https://doi.org/10.1029/2008jc004930

Chanard, K., Fleitout, L., Calais, E., Rebischung, P., & Avouac, J.-P. (2018). Toward a global horizontal and vertical elastic load deformation model derived from GRACE and GNSS station position time series. *Journal of Geophysical Research: Solid Earth*, *123*(4), 3225–3237. https://doi.org/10.1002/2017jb015245

Chen, J., Famiglietti, J. S., Scanlon, B. R., & Rodell, M. (2016). Groundwater storage changes: Present status from grace observations. In *Remote sensing and water resources* (pp. 207–227). Springer. https://doi.org/10.1007/978-3-319-32449-4_9

Chen, J., Rodell, M., Wilson, C., & Famiglietti, J. (2005). Low degree spherical harmonic influences on gravity recovery and climate experiment (GRACE) water storage estimates. *Geophysical Research Letters*, *32*(14), L14405. https://doi.org/10.1029/2005gl022964

Chen, J., Wilson, C., Blankenship, D., & Tapley, B. (2006). Antarctic mass rates from GRACE. *Geophysical Research Letters*, *33*(11), L11502. https://doi.org/10.1029/2006gl026369

Chen, J., Wilson, C., Famiglietti, J., & Rodell, M. (2007). Attenuation effect on seasonal basin-scale water storage changes from GRACE time-variable gravity. *Journal of Geodesy*, *81*(4), 237–245. https://doi.org/10.1007/s00190-006-0104-2

Chen, J., Wilson, C., Li, J., & Zhang, Z. (2015). Reducing leakage error in GRACE-observed long-term ice mass change: A case study in west Antarctica. *Journal of Geodesy*, *89*(9), 925–940. https://doi.org/10.1007/s00190-015-0824-2

Chen, J., Wilson, C., & Tapley, B. (2006). Satellite gravity measurements confirm accelerated melting of Greenland ice sheet. *Science*, *313*(5795), 1958–1960. https://doi.org/10.1126/science.1129007

Chen, J., Wilson, C., Tapley, B., Save, H., & Cretaux, J.-F. (2017). Long-term and seasonal Caspian sea level change from satellite gravity and altimeter measurements. *Journal of Geophysical Research: Solid Earth*, *122*(3), 2274–2290. https://doi.org/10.1002/2016jb013595

Chen, J. L., Wilson, C. R., Tapley, B. D., & Grand, S. (2007). GRACE detects coseismic and postseismic deformation from the Sumatra-Andaman earthquake. *Geophysical Research Letters*, *34*(13), L13302. https://doi.org/10.1029/2007gl030356

Cheng, M., Ries, J. C., & Tapley, B. D. (2011). Variations of the Earth's figure axis from satellite laser ranging and GRACE. *Journal of Geophysical Research*, *116*(B1), B01409. https://doi.org/10.1029/2010jb000850

De Viron, O., Diament, M., & Panet, I. (2006). Extracting low frequency climate signal from GRACE data. *eEarth Discussions*, *1*(1), 21–36. https://doi.org/10.5194/eed-1-21-2006

Dobslaw, H., Bergmann-Wolf, I., Dill, R., Poropat, L., Thomas, M., Dahle, C., et al. (2017). A new high-resolution model of non-tidal atmosphere and ocean mass variability for de-aliasing of satellite gravity observations: AOD1B RL06. *Geophysical Journal International*, *211*(1), 263–269. https://doi.org/10.1093/gji/ggx302

Dobslaw, H., Dill, R., Bagge, M., Klemann, V., Boergens, E., Thomas, M., et al. (2020). Gravitationally consistent mean Barystatic sea level rise from leakage-corrected monthly GRACE data. *Journal of Geophysical Research: Solid Earth*, *125*(11), e2020JB020923. https://doi.org/10.1029/2020jb020923

Dong, D., Fang, P., Bock, Y., Cheng, M., & Miyazaki, S. (2002). Anatomy of apparent seasonal variations from GPS-derived site position time series. *Journal of Geophysical Research*, *107*(B4), ETG-9. https://doi.org/10.1029/2001jb000573

Feng, W., Zhong, M., Lemoine, J.-M., Biancale, R., Hsu, H.-T., & Xia, J. (2013). Evaluation of groundwater depletion in north China using the gravity recovery and climate experiment (GRACE) data and ground-based measurements. *Water Resources Research*, *49*(4), 2110–2118. https://doi.org/10.1002/wrcr.20192

Flechtner, F., Neumayer, K.-H., Dahle, C., Dobslaw, H., Fagiolini, E., Raimondo, J.-C., & Güntner, A. (2016). What can be expected from the GRACE-FO laser ranging interferometer for Earth science applications? *Surveys in Geophysics*, *37*(2), 453–470. https://doi.org/10.1007/s10712-015-9338-y

Forootan, E., & Kusche, J. (2012). Separation of global time-variable gravity signals into maximally independent components. *Journal of Geodesy*, *86*(7), 477–497. https://doi.org/10.1007/s00190-011-0532-5

Forootan, E., Rietbroek, R., Kusche, J., Sharifi, M. A., Awange, J. L., Schmidt, M., et al. (2014). Separation of large scale water storage patterns over Iran using GRACE, altimetry and hydrological data. *Remote Sensing of Environment*, *140*, 580–595. https://doi.org/10.1016/j.rse.2013.09.025

Frappart, F., Ramillien, G., Leblanc, M., Tweed, S., Bonnet, M.-P., & Maisongrande, P. (2010). Continental water mass variations from independent component analysis (ICA) of level-2 monthly GRACE data. In *EGU general assembly conference abstracts* (p. 5873).

Gardner, A. S., Moholdt, G., Cogley, J. G., Wouters, B., Arendt, A. A., Wahr, J., et al. (2013). A reconciled estimate of glacier contributions to sea level rise: 2003 to 2009. *Science*, *340*(6134), 852–857. https://doi.org/10.1126/science.1234532

Ghil, M., Allen, M., Dettinger, M., Ide, K., Kondrashov, D., Mann, M., et al. (2002). Advanced spectral methods for climatic time series. *Reviews of Geophysics*, *40*(1), 3–1. https://doi.org/10.1029/2000rg000092

Guo, J., Duan, X., & Shum, C. (2010). Non-isotropic Gaussian smoothing and leakage reduction for determining mass changes over land and ocean using GRACE data. *Geophysical Journal International*, *181*(1), 290–302. https://doi.org/10.1111/j.1365-246x.2010.04534.x

Han, S.-C., Jekeli, C., & Shum, C. (2004). Time-variable aliasing effects of ocean tides, atmosphere, and continental water mass on monthly mean GRACE gravity field. *Journal of Geophysical Research*, *109*(B4), B04403. https://doi.org/10.1029/2003jb002501

Humphrey, V., & Gudmundsson, L. (2019). GRACE-REC: A reconstruction of climate-driven water storage changes over the last century. *Earth System Science Data*, *11*(3), 1153–1170. https://doi.org/10.5194/essd-11-1153-2019

Jäggi, A., Dahle, C., Arnold, D., Bock, H., Meyer, U., Beutler, G., & van Den Ijssel, J. (2016). Swarm kinematic orbits and gravity fields from 18 months of GPS data. *Advances in Space Research*, *57*(1), 218–233. https://doi.org/10.1016/j.asr.2015.10.035

Jäggi, A., Meyer, U., Lasser, M., Jenny, B., Lopez, T., Flechtner, F., et al. (2020). International combination service for time-variable gravity fields (COST-G) start of operational phase and future perspectives. In *Beyond 100: The next century in geodesy: Proceedings of the IAG General Assembly* (pp. 57–65). Montreal, Canada: Springer Cham International Publishing.

Jaguś, A., Rzętała, M. A., & Rzętała, M. (2015). Water storage possibilities in Lake Baikal and in reservoirs impounded by the dams of the Angara river cascade. *Environmental Earth Sciences*, *73*(2), 621–628. https://doi.org/10.1007/s12665-014-3166-0

Jeon, T., Seo, K.-W., Youm, K., Chen, J., & Wilson, C. R. (2018). Global sea level change signatures observed by GRACE satellite gravimetry. *Scientific Reports*, *8*(1), 1–10. https://doi.org/10.1038/s41598-018-31972-8

Johnson, G. C., & Chambers, D. P. (2013). Ocean bottom pressure seasonal cycles and decadal trends from GRACE release-05: Ocean circulation implications. *Journal of Geophysical Research: Oceans*, *118*(9), 4228–4240. https://doi.org/10.1002/jgrc.20307

Keppenne, C. L., & Ghil, M. (1993). Adaptive filtering and prediction of noisy multivariate signals: An application to subannual variability in atmospheric angular momentum. *International Journal of Bifurcation and Chaos*, *3*(03), 625–634. https://doi.org/10.1142/s0218127493000520

Klinger, B., & Mayer-Gürr, T. (2016). The role of accelerometer data calibration within GRACE gravity field recovery: Results from ITSG-GRACE2016. *Advances in Space Research*, *58*(9), 1597–1609. https://doi.org/10.1016/j.asr.2016.08.007

Kondrashov, D., & Ghil, M. (2006). Spatio-temporal filling of missing points in geophysical data sets. *Nonlinear Processes in Geophysics*, *13*(2), 151–159. https://doi.org/10.5194/npg-13-151-2006

Kondrashov, D., Shprits, Y., & Ghil, M. (2010). Gap filling of solar wind data by singular spectrum analysis. *Geophysical Research Letters*, *37*(15), L15101. https://doi.org/10.1029/2010gl044138

Kusche, J. (2007). Approximate decorrelation and non-isotropic smoothing of time-variable GRACE-type gravity field models. *Journal of Geodesy*, *81*(11), 733–749. https://doi.org/10.1007/s00190-007-0143-3

Kusche, J., Schmidt, R., Petrovic, S., & Rietbroek, R. (2009). Decorrelated GRACE time-variable gravity solutions by GFZ, and their validation using a hydrological model. *Journal of Geodesy*, *83*(10), 903–913. https://doi.org/10.1007/s00190-009-0308-3

Lai, Y., Zhang, B., Yao, Y., Liu, L., Yan, X., He, Y., & Ou, S. (2022). Reconstructing the data gap between GRACE and GRACE follow-on at the basin scale using artificial neural network. *Science of the Total Environment*, *823*, 153770. https://doi.org/10.1016/j.scitotenv.2022.153770

Landerer, F. W., Flechtner, F. M., Save, H., Webb, F. H., Bandikova, T., Bertiger, W. I., et al. (2020). Extending the global mass change data record: GRACE follow-on instrument and science data performance. *Geophysical Research Letters*, *47*(12), e2020GL088306. https://doi.org/10.1029/2020gl088306

Landerer, F. W., & Swenson, S. (2012). Accuracy of scaled GRACE terrestrial water storage estimates. *Water Resources Research*, *48*(4), W04531. https://doi.org/10.1029/2011wr011453

Larochelle, S., Chanard, K., Fleitout, L., Fortin, J., Gualandi, A., Longuevergne, L., et al. (2022). Understanding the geodetic signature of large aquifer systems: Example of the Ozark plateaus in central United States. *Journal of Geophysical Research: Solid Earth*, *127*(3), e2021JB023097. https://doi.org/10.1029/2021jb023097

Li, W., Wang, W., Zhang, C., Wen, H., Zhong, Y., Zhu, Y., & Li, Z. (2019). Bridging terrestrial water storage anomaly during GRACE/GRACE-FO gap using SSA method: A case study in China. *Sensors*, *19*(19), 4144. https://doi.org/10.3390/s19194144

Long, D., Longuevergne, L., & Scanlon, B. R. (2015). Global analysis of approaches for deriving total water storage changes from GRACE satellites. *Water Resources Research*, *51*(4), 2574–2594. https://doi.org/10.1002/2014wr016853

Longuevergne, L., Wilson, C., Scanlon, B., & Crétaux, J. (2013). GRACE water storage estimates for the Middle East and other regions with significant reservoir and lake storage. *Hydrology and Earth System Sciences*, *17*(12), 4817–4830. https://doi.org/10.5194/hess-17-4817-2013

Loomis, B., Luthcke, S., & Sabaka, T. (2019). Regularization and error characterization of GRACE mascons. *Journal of Geodesy*, *93*(9), 1381–1398. https://doi.org/10.1007/s00190-019-01252-y

Loomis, B., Rachlin, K. E., Wiese, D. N., Landerer, F. W., & Luthcke, S. B. (2020). Replacing GRACE/GRACE-FO with satellite laser ranging: Impacts on Antarctic ice sheet mass change. *Geophysical Research Letters*, *47*(3), e2019GL085488. https://doi.org/10.1029/2019gl085488

Lorenz, E. N. (1956). *Empirical orthogonal functions and statistical weather prediction* (Vol. 1). Massachusetts Institute of Technology, Department of Meteorology.

Lück, C., Kusche, J., Rietbroek, R., & Löcher, A. (2018). Time-variable gravity fields and ocean mass change from 37 months of kinematic swarm orbits. *Solid Earth*, *9*(2), 323–339. https://doi.org/10.5194/se-9-323-2018

Luthcke, S. B., Sabaka, T., Loomis, B., Arendt, A., McCarthy, J., & Camp, J. (2013). Antarctica, Greenland and Gulf of Alaska land-ice evolution from an iterated GRACE global mascon solution. *Journal of Glaciology*, *59*(216), 613–631. https://doi.org/10.3189/2013jog12j147

Mémin, A., Boy, J.-P., & Santamaría-Gómez, A. (2020). Correcting GPS measurements for non-tidal loading. *GPS Solutions*, *24*(2), 1–13. https://doi.org/10.1007/s10291-020-0959-3

Meyer, U., Jäggi, A., Jean, Y., & Beutler, G. (2016). AIUB-RL02: An improved time-series of monthly gravity fields from GRACE data. *Geophysical Journal International*, *205*(2), 1196–1207. https://doi.org/10.1093/gji/ggw081

Meyer, U., Jean, Y., Kvas, A., Dahle, C., Lemoine, J.-M., & Jäggi, A. (2019). Combination of GRACE monthly gravity fields on the normal equation level. *Journal of Geodesy*, *93*(9), 1645–1658. https://doi.org/10.1007/s00190-019-01274-6

Mo, S., Zhong, Y., Forootan, E., Mehrnegar, N., Yin, X., Wu, J., et al. (2022). Bayesian convolutional neural networks for predicting the terrestrial water storage anomalies during GRACE and GRACE-FO gap. *Journal of Hydrology*, *604*, 127244. https://doi.org/10.1016/j.jhydrol.2021.127244

Morison, J., Wahr, J., Kwok, R., & Peralta-Ferriz, C. (2007). Recent trends in Arctic Ocean mass distribution revealed by GRACE. *Geophysical Research Letters*, *34*(7), L07602. https://doi.org/10.1029/2006gl029016

Oh, T. H., Hasanuzzaman, M., Selvaraj, J., Teo, S. C., & Chua, S. C. (2018). Energy policy and alternative energy in Malaysia: Issues and challenges for sustainable growth–An update. *Renewable and Sustainable Energy Reviews*, *81*, 3021–3031. https://doi.org/10.1016/j.rser.2017.06.112

Oh, T. H., Pang, S. Y., & Chua, S. C. (2010). Energy policy and alternative energy in Malaysia: Issues and challenges for sustainable growth. *Renewable and Sustainable Energy Reviews*, *14*(4), 1241–1252. https://doi.org/10.1016/j.rser.2009.12.003

Panet, I., Mikhailov, V., Diament, M., Pollitz, F., King, G., De Viron, O., et al. (2007). Coseismic and post-seismic signatures of the Sumatra 2004 December and 2005 march earthquakes in GRACE satellite gravity. *Geophysical Journal International*, *171*(1), 177–190. https://doi.org/10.1111/j.1365-246x.2007.03525.x

Peltier, W. R., Argus, D., & Drummond, R. (2015). Space geodesy constrains ice age terminal deglaciation: The global ice-6G_C (VM5a) model. *Journal of Geophysical Research: Solid Earth*, *120*(1), 450–487. https://doi.org/10.1002/2014jb011176

Peltier, W. R., Argus, D. F., & Drummond, R. (2018). Comment on "an assessment of the ice-6G_C (VM5a) glacial isostatic adjustment model" by Purcell et al. *Journal of Geophysical Research: Solid Earth*, *123*(2), 2019–2028. https://doi.org/10.1002/2016jb013844

Plaut, G., & Vautard, R. (1994). Spells of low-frequency oscillations and weather regimes in the northern hemisphere. *Journal of the Atmospheric Sciences*, *51*(2), 210–236. https://doi.org/10.1175/1520-0469(1994)051<0210:solfoa>2.0.co;2

Prevost, P., Chanard, K., Fleitout, L., Calais, E., Walwer, D., van Dam, T., & Ghil, M. (2019). Data-adaptive spatio-temporal filtering of GRACE data. *Geophysical Journal International*, *219*(3), 2034–2055. https://doi.org/10.1093/gji/ggz409

Rangelova, E., Sideris, M., & Kim, J. (2012). On the capabilities of the multi-channel singular spectrum method for extracting the main periodic and non-periodic variability from weekly GRACE data. *Journal of Geodynamics*, *54*, 64–78. https://doi.org/10.1016/j.jog.2011.10.006

Rangelova, E., & Sideris, M. G. (2008). Contributions of terrestrial and GRACE data to the study of the secular geoid changes in North America. *Journal of Geodynamics*, *46*(3–5), 131–143. https://doi.org/10.1016/j.jog.2008.03.006

Rangelova, E., Van der Wal, W., Braun, A., Sideris, M., & Wu, P. (2007). Analysis of gravity recovery and climate experiment time-variable mass redistribution signals over North America by means of principal component analysis. *Journal of Geophysical Research*, *112*(F3), F03002. https://doi.org/10.1029/2006jf000615

Richter, H. M. P., Lück, C., Klos, A., Sideris, M. G., Rangelova, E., & Kusche, J. (2021). Reconstructing GRACE-type time-variable gravity from the swarm satellites. *Scientific Reports*, *11*(1), 1–14. https://doi.org/10.1038/s41598-020-80752-w

Rieser, D., Kuhn, M., Pail, R., Anjasmara, I., & Awange, J. (2010). Relation between GRACE-derived surface mass variations and precipitation over Australia. *Australian Journal of Earth Sciences*, *57*(7), 887–900. https://doi.org/10.1080/08120099.2010.512645

Rietbroek, R., Fritsche, M., Dahle, C., Brunnabend, S.-E., Behnisch, M., Kusche, J., et al. (2014). Can GPS-derived surface loading bridge a GRACE mission gap? *Surveys in Geophysics*, *35*(6), 1267–1283. https://doi.org/10.1007/s10712-013-9276-5

Rodell, M., Chen, J., Kato, H., Famiglietti, J. S., Nigro, J., & Wilson, C. R. (2007). Estimating groundwater storage changes in the Mississippi River basin (USA) using GRACE. *Hydrogeology Journal*, *15*(1), 159–166. https://doi.org/10.1007/s10040-006-0103-7

Rodell, M., Houser, P., Jambor, U., Gottschalck, J., Mitchell, K., Meng, C.-J., et al. (2004). The global land data assimilation system. *Bulletin of the American Meteorological Society*, *85*(3), 381–394. https://doi.org/10.1175/bams-85-3-381

Sakumura, C., Bettadpur, S., & Bruinsma, S. (2014). Ensemble prediction and intercomparison analysis of GRACE time-variable gravity field models. *Geophysical Research Letters*, *41*(5), 1389–1397. https://doi.org/10.1002/2013gl058632

Save, H., Bettadpur, S., & Tapley, B. D. (2012). Reducing errors in the GRACE gravity solutions using regularization. *Journal of Geodesy*, *86*(9), 695–711. https://doi.org/10.1007/s00190-012-0548-5

Save, H., Bettadpur, S., & Tapley, B. D. (2016). High-resolution CSR GRACE RL05 mascons. *Journal of Geophysical Research: Solid Earth*, *121*(10), 7547–7569. https://doi.org/10.1002/2016jb013007

Scanlon, B. R., Longuevergne, L., & Long, D. (2012). Ground referencing GRACE satellite estimates of groundwater storage changes in the California central valley, USA. *Water Resources Research*, *48*(4), W04520. https://doi.org/10.1029/2011wr011312

Schrama, E. J., Wouters, B., & Lavallée, D. A. (2007). Signal and noise in gravity recovery and climate experiment (GRACE) observed surface mass variations. *Journal of Geophysical Research*, *112*(B8), B08407. https://doi.org/10.1029/2006jb004882

Seo, K.-W., Wilson, C., Famiglietti, J., Chen, J., & Rodell, M. (2006). Terrestrial water mass load changes from gravity recovery and climate experiment (GRACE). *Water Resources Research*, *42*(5), W05417. https://doi.org/10.1029/2005wr004255

Seo, K.-W., Wilson, C. R., Chen, J., & Waliser, D. E. (2007). GRACE's spatial aliasing error. *Geophysical Journal International*, *172*(1), 41–48. https://doi.org/10.1111/j.1365-246x.2007.03611.x

Sośnica, K., Jäggi, A., Meyer, U., Thaller, D., Beutler, G., Arnold, D., & Dach, R. (2015). Time variable Earth's gravity field from SLR satellites. *Journal of Geodesy*, *89*(10), 945–960. https://doi.org/10.1007/s00190-015-0825-1

Steffen, H., Denker, H., & Müller, J. (2008). Glacial isostatic adjustment in Fennoscandia from GRACE data and comparison with geodynamical models. *Journal of Geodynamics*, *46*(3–5), 155–164. https://doi.org/10.1016/j.jog.2008.03.002

Sun, Y., Riva, R., & Ditmar, P. (2016). Optimizing estimates of annual variations and trends in geocenter motion and J_2 from a combination of GRACE data and geophysical models. *Journal of Geophysical Research: Solid Earth*, *121*(11), 8352–8370. https://doi.org/10.1002/2016jb013073

Swenson, S., Chambers, D., & Wahr, J. (2008). Estimating geocenter variations from a combination of GRACE and ocean model output. *Journal of Geophysical Research*, *113*(B8), B08410. https://doi.org/10.1029/2007jb005338

Swenson, S., & Wahr, J. (2002). Methods for inferring regional surface-mass anomalies from gravity recovery and climate experiment (GRACE) measurements of time-variable gravity. *Journal of Geophysical Research*, *107*(B9), ETG-3–ETG-13. https://doi.org/10.1029/2001jb000576

Swenson, S., & Wahr, J. (2006). Post-processing removal of correlated errors in GRACE data. *Geophysical Research Letters*, *33*(8), L08402. https://doi.org/10.1029/2005gl025285

Swenson, S., & Wahr, J. (2007). Multi-sensor analysis of water storage variations of the Caspian Sea. *Geophysical Research Letters*, *34*(16), L16401. https://doi.org/10.1029/2007gl030733

Syed, T. H., Famiglietti, J. S., Rodell, M., Chen, J., & Wilson, C. R. (2008). Analysis of terrestrial water storage changes from GRACE and GLDAS. *Water Resources Research*, *44*(2), W02433. https://doi.org/10.1029/2006wr005779

Tangdamrongsub, N., Han, S.-C., Jasinski, M. F., & Šprlák, M. (2019). Quantifying water storage change and land subsidence induced by reservoir impoundment using GRACE, Landsat, and GPS data. *Remote Sensing of Environment*, *233*, 111385. https://doi.org/10.1016/j.rse.2019.111385

Tapley, B. D., Bettadpur, S., Ries, J. P., Thompson, P. F., & Watkins, M. M. (2004). GRACE measurements of mass variability in the Earth system. *Science*, *305*(5683), 503–505. https://doi.org/10.1126/science.1099192

Teixeira da Encarnação, J., Arnold, D., Bezděk, A., Dahle, C., Doornbos, E., Van Den Ijssel, J., et al. (2016). Gravity field models derived from swarm GPS data. *Earth, Planets and Space*, *68*(1), 1–15. https://doi.org/10.1186/s40623-016-0499-9

Teixeira da Encarnação, J., Visser, P., Arnold, D., Bezdek, A., Doornbos, E., Ellmer, M., et al. (2020). Description of the multi-approach gravity field models from swarm GPS data. *Earth System Science Data*, *12*(2), 1385–1417. https://doi.org/10.5194/essd-12-1385-2020

Thompson, P., Bettadpur, S., & Tapley, B. (2004). Impact of short period, non-tidal, temporal mass variability on GRACE gravity estimates. *Geophysical Research Letters*, *31*(6), L06619. https://doi.org/10.1029/2003gl019285

Velicogna, I., & Wahr, J. (2013). Time-variable gravity observations of ice sheet mass balance: Precision and limitations of the GRACE satellite data. *Geophysical Research Letters*, *40*(12), 3055–3063. https://doi.org/10.1002/grl.50527

Vianna, M. L., Menezes, V. V., & Chambers, D. P. (2007). A high resolution satellite-only GRACE-based mean dynamic topography of the South Atlantic Ocean. *Geophysical Research Letters*, *34*(24), L24604. https://doi.org/10.1029/2007gl031912

Vishwakarma, B. D., Horwath, M., Devaraju, B., Groh, A., & Sneeuw, N. (2017). A data-driven approach for repairing the hydrological catchment signal damage due to filtering of GRACE products. *Water Resources Research*, *53*(11), 9824–9844. https://doi.org/10.1002/2017wr021150

Wahr, J., Swenson, S., Zlotnicki, V., & Velicogna, I. (2004). Time-variable gravity from GRACE: First results. *Geophysical Research Letters*, *31*(11), L11501. https://doi.org/10.1029/2004gl019779

Walwer, D., Calais, E., & Ghil, M. (2016). Data-adaptive detection of transient deformation in geodetic networks. *Journal of Geophysical Research: Solid Earth*, *121*(3), 2129–2152. https://doi.org/10.1002/2015jb012424

Wang, F., Shen, Y., Chen, Q., & Wang, W. (2021). Bridging the gap between GRACE and GRACE follow-on monthly gravity field solutions using improved multichannel singular spectrum analysis. *Journal of Hydrology*, *594*, 125972. https://doi.org/10.1016/j.jhydrol.2021.125972

Wang, F., Shen, Y., Chen, T., Chen, Q., & Li, W. (2020). Improved multichannel singular spectrum analysis for post-processing GRACE monthly gravity field models. *Geophysical Journal International*, *223*(2), 825–839. https://doi.org/10.1093/gji/ggaa339

Wang, X., de Linage, C., Famiglietti, J., & Zender, C. S. (2011). Gravity recovery and climate experiment (GRACE) detection of water storage changes in the three gorges reservoir of China and comparison with in situ measurements. *Water Resources Research*, *47*(12), W12502. https://doi.org/10.1029/2011wr010534

Watkins, M. M., Wiese, D. N., Yuan, D.-N., Boening, C., & Landerer, F. W. (2015). Improved methods for observing Earth's time variable mass distribution with GRACE using spherical cap mascons. *Journal of Geophysical Research: Solid Earth*, *120*(4), 2648–2671. https://doi.org/10.1002/2014jb011547

Werth, S., Güntner, A., Schmidt, R., & Kusche, J. (2009). Evaluation of GRACE filter tools from a hydrological perspective. *Geophysical Journal International*, *179*(3), 1499–1515. https://doi.org/10.1111/j.1365-246x.2009.04355.x

Wouters, B., Chambers, D., & Schrama, E. (2008). GRACE observes small-scale mass loss in Greenland. *Geophysical Research Letters*, *35*(20), L20501. https://doi.org/10.1029/2008gl034816

Wouters, B., Gardner, A. S., & Moholdt, G. (2019). Global glacier mass loss during the GRACE satellite mission (2002-2016). *Frontiers in Earth Science*, *7*, 96. https://doi.org/10.3389/feart.2019.00096

Wouters, B., Riva, R., Lavallée, D., & Bamber, J. (2011). Seasonal variations in sea level induced by continental water mass: First results from GRACE. *Geophysical Research Letters*, *38*(3), L03303. https://doi.org/10.1029/2010gl046128

Wouters, B., & Schrama, E. J. (2007). Improved accuracy of GRACE gravity solutions through empirical orthogonal function filtering of spherical harmonics. *Geophysical Research Letters*, *34*(23), L23711. https://doi.org/10.1029/2007gl032098

Wu, X., Haines, B. J., Heflin, M. B., & Landerer, F. W. (2020). Improved global nonlinear surface mass variation estimates from geodetic displacements and reconciliation with GRACE data. *Journal of Geophysical Research: Solid Earth*, *125*(2), e2019JB018355. https://doi.org/10.1029/2019jb018355

Yang, X., Tian, S., You, W., & Jiang, Z. (2021). Reconstruction of continuous GRACE/GRACE-FO terrestrial water storage anomalies based on time series decomposition. *Journal of Hydrology*, *603*, 127018. https://doi.org/10.1016/j.jhydrol.2021.127018

Yi, S., & Sneeuw, N. (2021). Filling the data gaps within GRACE missions using singular spectrum analysis. *Journal of Geophysical Research: Solid Earth*, *126*(5), e2020JB021227. https://doi.org/10.1029/2020jb021227

Zotov, L., & Shum, C. (2010). Multichannel singular spectrum analysis of the gravity field data from GRACE satellites. In *AIP conference proceedings* (Vol. 1206, pp. 473–479). https://doi.org/10.1063/1.3292557

References From the Supporting Information

Allen, M., & Robertson, A. (1996). Distinguishing modulated oscillations from coloured noise in multivariate datasets. *Climate Dynamics*, *12*(11), 775–784. https://doi.org/10.1007/s003820050142

Broomhead, D. S., & King, G. P. (1986). Extracting qualitative dynamics from experimental data. *Physica D: Nonlinear Phenomena*, *20*(2–3), 217–236. https://doi.org/10.1016/0167-2789(86)90031-x

Broomhead, D. S., & King, G. P. (1986). On the qualitative analysis of experimental dynamical systems. *Nonlinear Phenomena and Chaos*, *113*, 114.